PERGAMON

Journal of Structural Geology 24 (2002) 1805–1828

JOURNAL OF STRUCTURAL GEOLOGY

www.elsevier.com/locate/jstrugeo

The tectonometamorphic evolution of high-pressure low-temperature metamorphic rocks of eastern Crete, Greece: constraints from microfabrics, strain, illite crystallinity and paleodifferential stress

G. Zulauf[a,*], G. Kowalczyk[b], J. Krahl[c], R. Petschick[b], S. Schwanz[b]

[a]*Institut für Geologie und Mineralogie, Universität Erlangen-Nürnberg, Schloβgarten 5, D-91054 Erlangen, Germany*
[b]*Geologisch-Paläontologisches Institut, Universität Frankfurt a.M., Senckenberganlage 32-34, D-60054 Frankfurt a.M., Germany*
[c]*Agnesstraβe 45, D-80798 München, Germany*

Received 28 March 2001; revised 27 November 2001; accepted 10 December 2001

Abstract

Analysis of strain, paleodifferential stress, illite crystallinity, and microfabrics of quartz and calcite suggest that multiply alternating late Oligocene/early Miocene N–S convergence and N–S extension caused significant vertical discontinuities in the grade of high-pressure/low-temperature metamorphism of the Phyllite–Quartzite unit (PQU) of eastern Crete. Constrictional fabrics and parallelism of D_2 stretching lineations and fold axes are attributed to enhanced slab pull forces at greater depth of subduction. A major D_3 extensional detachment is present in the upper part of the PQU where slates with lowest metamorphic grade (diagenesis/anchizone transition) are resting on top of anchimetamorphic rocks. The highest metamorphic grade (anchi-/epizone transition) has been determined for Skythian rocks on top of pre-Alpine basement. Revived N–S convergence (D_4) led to E–W-trending map-scale folds and top-to-the-S directed brittle thrusts. There is a clear correlation between D_2-related metamorphic grade, finite strain, differential stress, and deformation mechanisms. At the anchi-/epizone transition, solution–precipitation and dislocation creep of quartz and calcite caused maximum finite strains (R_{XZ} = up to 7) at high strain rates and moderate differential stresses (80–200 MPa). At the diagenesis/anchizone transition, deformation was accommodated by cataclasis, dislocation glide and solution–precipitation creep resulting in relatively low finite strains ($R_{XZ} < 2$) at high differential stresses of up to 300 MPa.

Keywords: Crete; Subduction; Deformation mechanisms quartz; Rheology; Strain analysis

1. Introduction

Subduction of continental crust is commonly associated with complex deformation, starting with thrusting and accretion under relatively high pressures and low temperatures, and ceasing with extensional unroofing at retrograde metamorphic conditions (e.g. Lister et al., 1984; Andersen and Jamtveit, 1990). The present paper describes such a scenario and presents constraints on the rheology of high-pressure/low-temperature metamorphic rocks of the Phyllite–Quartzite and the Plattenkalk unit of eastern Crete. Paleodifferential stress, finite strain, microfabrics and illite crystallinity have been determined with respect to the most pervasive, subduction-related deformation event. These data vary significantly along the tectonostratigraphic sequence of the PQU suggesting vertical changes in the metamorphic grade due to post-peak metamorphic extensional shearing and thrusting. It will be shown that changes in the peak-metamorphic temperature, from the diagenesis/anchizone to the anchi-/epizone transition, causes remarkable changes in rheology, which are reflected by deformation mechanisms, differential stress and finite strain.

The reconstruction of the individual structural events and related metamorphic temperatures, starting with subduction/collision and ceasing with exhumation, is documented in detail by the geometry and microfabrics of quartz fibers that grew in pressure shadows of pyrite. It will be shown that subduction of continental crust may result in prolate coaxial and noncoaxial fabrics that differ considerably from those of common foreland fold/thrust belts.

2. Regional geology

The island of Crete forms a horst within the 'fore-arc'

* Corresponding author. Tel.: +49-9131-85-22617; fax: +49-9131-85-29295.
E-mail address: zulauf@geol.uni-erlangen.de (G. Zulauf).

0191-8141/02/$ - see front matter
PII: S0191-8141(01)00168-7

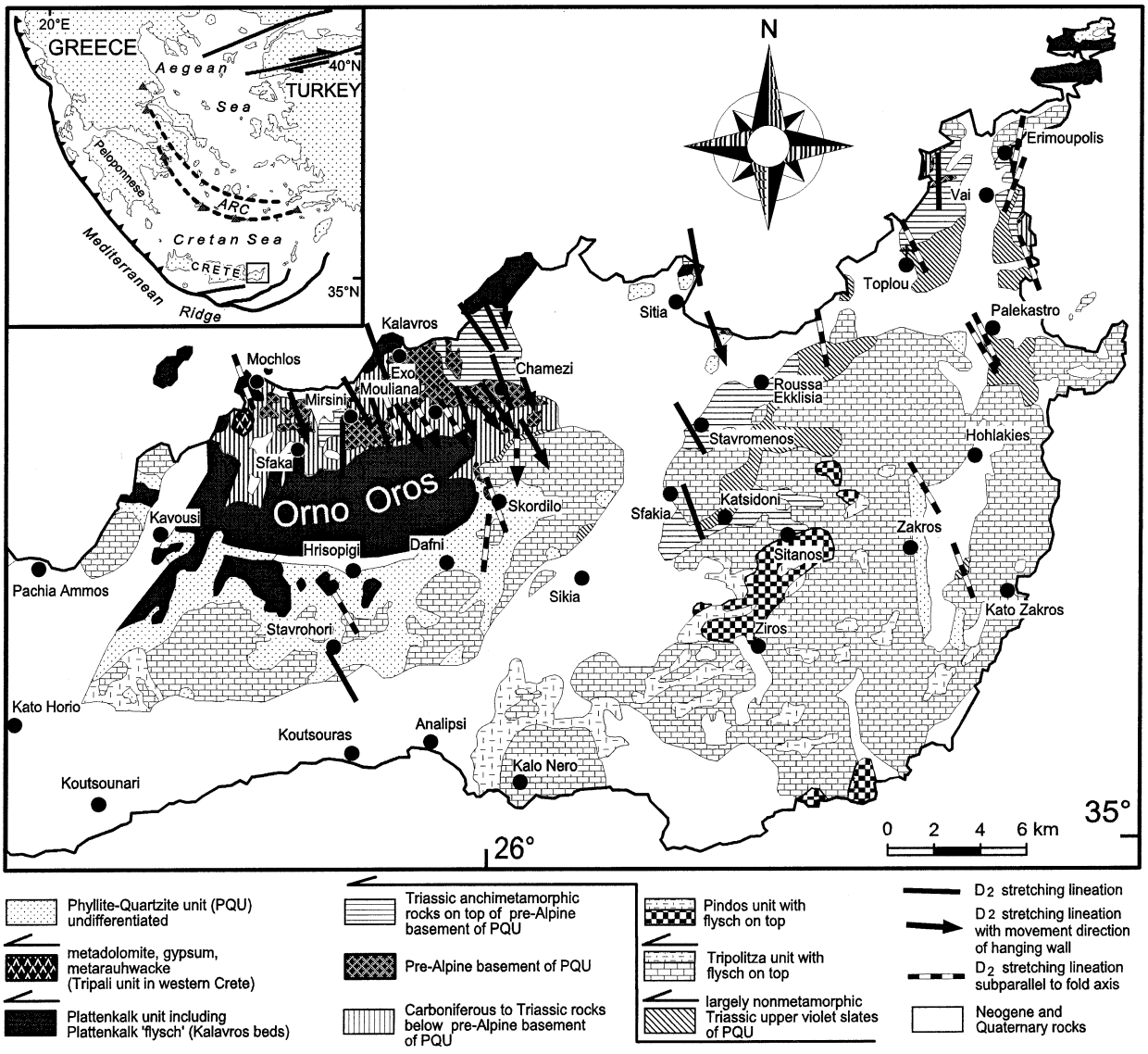

Fig. 1. Geological map of eastern Crete (compiled after Creutzburg and Seidel, 1975; Seidel et al., 1982; Krahl et al., 1986; Haude, 1989; Franz, 1992; Dornsiepen and Manutsoglu, 1994; and own data) with direction of D_2 fold axes and D_2 stretching lineation.

region above the active northward-directed subduction of the African plate. Apart from subduction, collision with a microcontinent has controlled the tectonometamorphic evolution of the pre-Neogene nappes of Crete at least since the Eocene (e.g. Wortel et al., 1993). According to their tectonometamorphic evolution and tectonostratigraphic position, the Cretan nappes can be subdivided into a lower and an upper group (Seidel et al., 1982). The *lower nappes* consist of the Permian to Oligocene Plattenkalk unit, the Triassic to Lower Jurassic Tripali unit, and the Carboniferous to Triassic Phyllite–Quartzite unit (Fig. 1), all of which have been affected by Oligocene/early Miocene high pressure/low temperature metamorphism (300–400 °C, 800–1000 MPa; Seidel et al., 1982; Theye et al., 1992; Theye and Seidel, 1993) and related deformation (e.g. Wachendorf et al., 1975; Greiling, 1982; Fassoulas et al., 1994; Kilias et al., 1994; Stöckhert et al., 1999). The Plattenkalk unit represents the most external Hellenic nappe.

The *upper nappes* include the Triassic to Eocene Tripolitza and Pindos units as well as the 'Uppermost' ophiolite- and melange-bearing unit, where Cretaceous metamorphism has been detected (Seidel et al., 1981). Within the upper nappes records of the Oligocene/early Miocene metamorphism have as yet not been detected. The boundary between the lower and the upper nappes, i.e. between the Phyllite–Quartzite and the Tripolitza unit, is interpreted as an extensional detachment (Fassoulas et al., 1994; Kilias et al., 1994; Jolivet et al., 1996).

Based on metamorphic index minerals in metapelites and on the stability of aragonite, the metamorphic peak in the Phyllite–Quartzite unit of western Crete has been

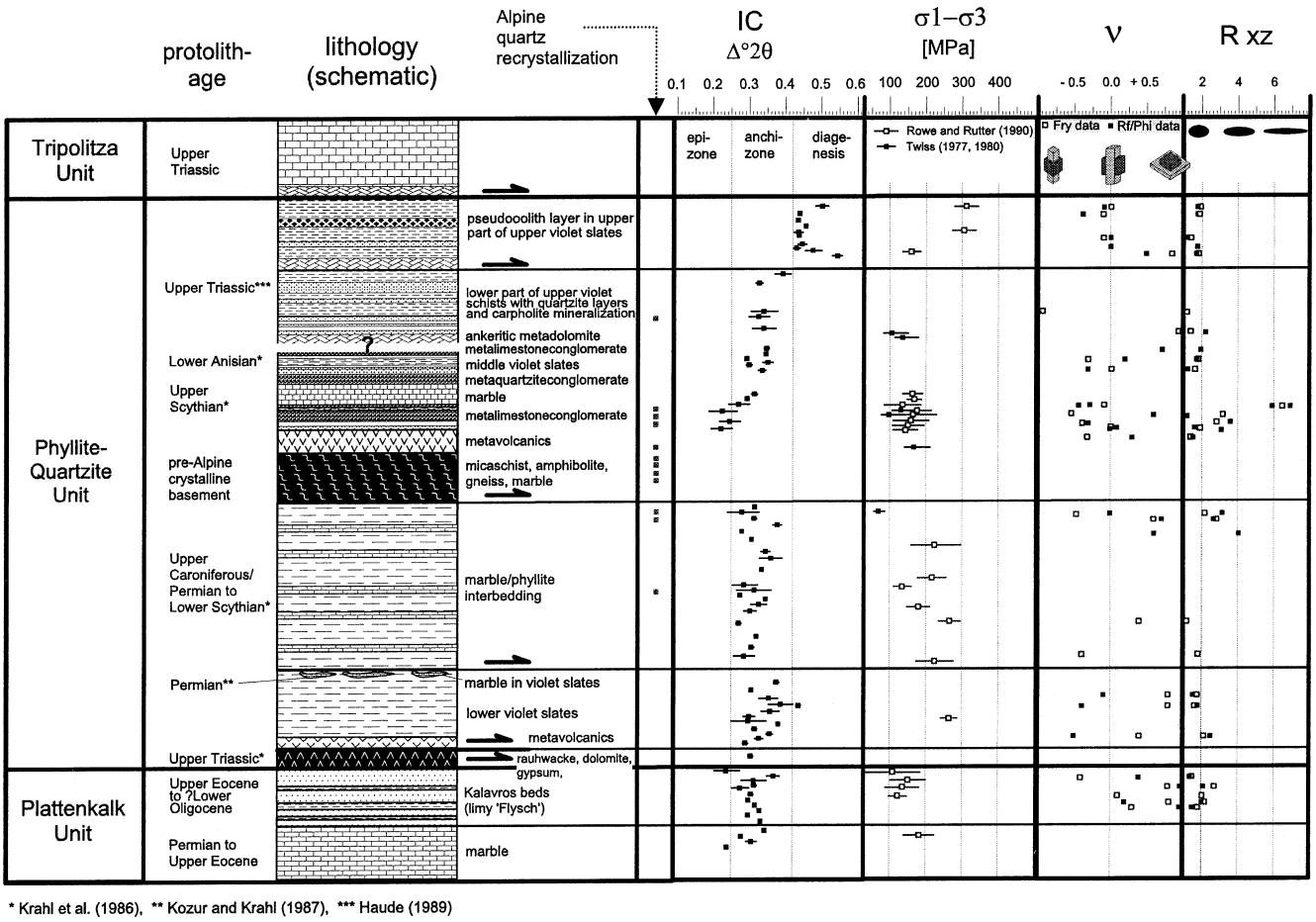

Fig. 2. Tectonostratigraphic sequence, illite crystallinity (IC), paleodifferential stress ($\sigma_1 - \sigma_3$), strain geometry (ν) and strain magnitude (R_{XZ}) of the Phyllite–Quartzite unit and the uppermost part of the Plattenkalk unit of eastern Crete (for further explanation see text).

determined at 1000 ± 200 MPa and 400 ± 50 °C (Theye and Seidel, 1991, 1993). The age of the metamorphic peak has been constrained to the period between 24 and 19 Ma using K–Ar and Ar–Ar ages of white mica (Seidel et al., 1982; Jolivet et al., 1996). As is indicated by fluid inclusions (Küster and Stöckhert, 1997) and fission-track data of zircon and apatite (Thomson et al., 1998a,b) exhumation and cooling to T = ca. 300 °C was nearly isothermal and should have been completed before 19 Ma, whereas the 100 °C isotherm was passed at ca. 15 Ma.

Latest compressional tectonics, related to subduction and associated crustal thickening, is poorly dated. The late Miocene extensional tectonics are commonly attributed to southward trench retreat (roll back) driven by the pull of the African slab (Le Pichon et al., 1982; Meulenkamp et al., 1988) and by westward movements of the Anatolian block along the North Anatolian Fault (Taymaz et al., 1991). Based on the thermal history of both the Phyllite–Quartzite and the Uppermost unit, Thomson et al. (1998b) argue that the Hellenic subduction zone acted as a retreating plate boundary much earlier, at least since the late Eocene.

3. The Phyllite–Quartzite unit of eastern Crete

In eastern Crete the Phyllite–Quartzite unit (PQU) is well exposed N and S of the Orno Oros, the core of which consists of rocks of the Plattenkalk unit (Fig. 1). Further exposures of the PQU are present near Sitia, Roussa Ekklisia, and between Erimoupolis and Zakros. Because of several tectonic contacts within the PQU, the sequence is referred to as a tectonostratigraphic sequence that is schematically depicted in Fig. 2. Particularly within the upper part of the PQU some members are completely lacking because of intense Alpine extensional tectonics.

The PQU of eastern Crete is characterized by a pre-Alpine crystalline basement (micaschist, gneiss, amphibolite and marble) that is well exposed north of the Orno Oros (Fig. 1). The basement and its Triassic cover have been thrust over Upper Carboniferous to Triassic rocks of the PQU (Krahl et al., 1986; Dornsiepen and Manutsoglu, 1994).

The sequence below the basement can be divided into three tectonic subunits. Above the Paleogene Kalavros beds, which are by some authors interpreted as Plattenkalk

flysch, metadolomite, metarauhwacke and gypsum occur in which Triassic fossils have been found (Krahl et al., 1986). The boundary to the overlying lower violet slates should be a thrust contact, as these slates are older. They include marbles with Permian fossils (Kozur and Krahl, 1987). Another thrust contact should exist between the lower violet slates and the overlying marble–phyllite interbedding where findings of fossils reflect Upper Carboniferous to Lower Skythian ages (Krahl et al., 1986). These rocks have been overthrust by the pre-Alpine basement. North of the Orno Oros, the Triassic variegated sequence on top of the pre-Alpine basement includes metavolcanics, metasandstone, metaconglomerate, marble, middle violet slates and upper violet slates. The contact between the upper violet slates and the overlying Tripolitza unit is always of tectonic origin.

The degree of Alpine metamorphism of the PQU of eastern Crete is less than in western Crete as is indicated by values of illite crystallinity and metamorphic index minerals that include pyrophyllite, chlorite, paragonite–illite mixed layers, Fe-carpholite, sudoite, lawsonite, and pumpellyite (Seidel et al., 1982; Theye et al., 1992). The P–T conditions have been roughly determined at 300 ± 50 °C and 800 ± 300 MPa (Theye et al., 1992). Similar values ($T = 250$–310 °C and $P = 450$–600 MPa) have been derived by Franz (1992). The exhumation of the subducted rocks was isothermal as is indicated by relatively low pressures ($P = 110$–230 MPa) at still high temperatures ($T = 270$–320 °C; Franz, 1992). Oxygen iostopes of quartz–carpholite veins yield temperatures around 250 °C (Stüben and Berner, 1999).

Existing structural data of eastern Crete include E–W-trending folds and shear zones that show top-to-the-S sense of shear (Wachendorf et al., 1975; Krahl et al., 1986; Haude, 1989; Franz, 1992).

4. Methods

To detect gradients and breaks in metamorphic grade along the tectonostratigraphic profile described above, *illite crystallinity* and *metamorphic index minerals*, such as kaolinite, paragonite–illite mixed layers, pyrophyllite, paragonite, Fe-carpholite have been determined from 135 samples using X-ray diffraction. Samples were first crushed using a mortar and then dispersed in diluted formic acid. After multiple washing, the rock powder was treated with Na-polyphosphate to prevent it from coagulation. For the separation of the fine fraction (<2 μm) the conventional Atterberg method was used. This separation is important to minimize the influence of detrital micas. From every sample two special specimens with high degree of oriented particles and defined specimen thickness (4 mg cm^{-2}) were produced that have been multiply measured. To assess the individual temperature regimes (diagenesis, anchizone, epizone) we used the data of Kübler (cf. Ferreiro Mählmann, 1994). Values for the boundaries diagenesis/anchizone and anchi-/epizone are set at 0.42 and 0.25 $\Delta°2\theta$ Cu Kα (cf. Frey, 1988; Fig. 2). The temperatures for these boundaries have been constrained at ca. 235 and 300 °C, respectively (Ferreiro Mählmann, 1994).

We further investigated the *microfabrics* using more than 200 thin sections to reconstruct the deformation sequence, the kinematics, the deformation–crystallization relations, and the deformation mechanisms of quartz and calcite. Apart from conventional microscopy with a petrological microscope, we applied the *cathodoluminescence technique* in cases of deformed marble.

Most tectonites of the PQU of eastern Crete contain suitable marker grains from which the *finite strain* can be determined. In some cases it was also possible to calculate the volumetric strain and determine individual strain increments using quartz fibers that grew in pressure shadows of rigid pyrite cubes. The particle strain was determined using the R_f/ϕ method (cf. Ramsay and Huber, 1983, p. 73). Analysed particles were pebbles of metaconglomerates or 'pseudoooids' of the upper violet slates. The matrix strains of (meta)siltstones, sandstones and fine-grained conglomerates were calculated with the traditional Fry or normalized Fry methods (Fry, 1979; Erslev, 1988). The strain was determined in XZ and YZ sections of the finite strain ellipsoid using the image-analysis software 'DIAna' (Duyster, 1991) and the program 'STRAIN' (Unzog, 1990). The latter calculates the conventional and normalized Fry strains as well as the R_f/ϕ strain after Ramsay and Huber (1983) and Peach and Lisle (1979). At least 40 and 300 particles were analysed when using the R_f/ϕ and Fry method, respectively.

Apart from the ellipticity of the finite strain ellipsoid of the principal sections (R_{xz}, R_{xy}, R_{yz}), the extension (e_x) along the X-axis of the finite strain ellipsoid could be determined in a few cases. From the amounts of R_{xz}, R_{xy}, R_{yz} and e_x we can calculate e_y and e_z. Given that the R_f/ϕ and Fry strain is similar, the volumetric strain can be determined according to the equation:

$$1 + \Delta V = (1 + e_x)(1 + e_y)(1 + e_z) \quad (1)$$

(Ramsay and Huber, 1983). To characterize the geometry of the finite strain ellipsoid, we calculated the k-value and the Lode's parameter, ν. To get quantitative data of the strain magnitude, we calculated the strain intensity (ϵ_s) after Nadai (1963). To determine the *differential stress* ($\sigma_1 - \sigma_3$) related to the most important and pervasive deformation event, we used two different paleopiezometers, one of which is based on the dynamically recrystallized grain size of quartz (Twiss, 1977), the other on the amount of twin lamellae per unit length in calcite (Rowe and Rutter, 1990). Twiss (1977) has shown the following relation between stress difference and recrystallized grain size:

$$(\sigma_1 - \sigma_3) = K\mu\mathbf{B}d^{-r} \quad (2)$$

where μ is the shear modulus, **B** is the Burgers vector, and K and r are empirically derived constants (cf. also Twiss and

Moores, 1992, p. 412). Main prerequisites for the application of the recrystallized grain-size piezometer are: (1) the growth of the recrystallized grains should not be influenced by other phases, (2) the recrystallized grains must reflect a steady-state deformation, and (3) static annealing should not occur subsequent to the formation of the recrystallized grains. It has to be noted that subgrain-rotation recrystallization yields smaller grains than high-temperature migration recrystallization (Guillope and Poirier, 1979; cf. also Twiss and Moores, 1992, p. 412). In the present case of the PQU of eastern Crete, we are dealing with low-temperature migration recrystallization (deformation regime 1 of Hirth and Tullis, 1992) that probably yields smaller grains than subgrain-rotation recrystallization (Zulauf, 2001). According to Hirth and Tullis (1992) recrystallized grains that result from migration recrystallization are more suitable for paleopiezometry than those grains that were formed during subgrain rotation.

As most of the grains show irregular shapes, we determined the diameter from the grain area that was measured using the image-analyses system DiAna (see above). For every sample at least 100 grains were analyzed to calculate the mean grain size and the standard deviation. Apart from the calibration of Twiss (1977, 1980), we used other calibrations after Mercier et al. (1977), White (1979), Etheridge and Wilkie (1981), Koch (1983) and Ord and Christie (1984).

The calcite-twin piezometer of Rowe and Rutter (1990) is based on the equation

$$(\sigma_1 - \sigma_3) = -52.0 + 171\log D \quad (3)$$

where D is the amount of twin lamellae in calcite per defined length. The calibration was performed at $T > 400$ °C where type III and IV twins developed according to the classification of Burkhard (1993). Thus, naturally deformed calcite grains that show such types of twin lamellae are most suitable for being applied for piezometry (cf. Rowe and Rutter, 1990). In our case, the twins of at least 50 calcite grains were counted under the microscope. We further measured the long and short axis of every grain to calculate its mean diameter. The latter was used to relate the amount of twins to the defined length.

5. Results

5.1. Illite crystallinity and metamorphic index minerals

Illite crystallinity (IC) data have been determined from metapelite, metatuffite and impure marble of the PQU. Further analyses concern some marbles of the Plattenkalk unit and pelitic parts of the Plattenkalk flysch (Kalavros beds). The investigations of the Plattenkalk unit have been carried out to compare our results with IC data derived by Soujon and Jacobshagen (1997) from the Plattenkalk of the Orno Oros. In cases where paragonite has been determined beside illite, the paragonite peak was eliminated using our computer-aided peak-fit method (Pearson VII splitted). Large amounts of paragonite–illite mixed layers have been frequently found in the upper violet slates below the Tripolitza unit. They might result in significant peak widening that cannot be treated by the peak-fit method. This is the reason why in Fig. 2 IC data are presented only from those samples where paragonite–illite mixed layers have not been detected. Further IC data that might be affected by illite–paragonite mixed layer minerals are listed in Table 1. These data show the mean values and standard deviation of at least three measurements.

The highest IC values occur in the upper part of the upper violet slates. Although these slates are situated close to the overlying Tripolitza carbonates, the analyzed samples do not show records of pervasive cataclastic deformation and related fluid-controlled alteration. The data plot at the diagenesis–anchizone transition ($\Delta°2\theta$ = around 0.45; Fig. 2), which is compatible with the fact that both kaolinite and pyrophyllite (or paragonite) as well as large amounts of paragonite–illite mixed layers have been detected. It has to be emphasized that paragonite–illite mixed layers are entirely restricted to this part of the PQU, but do not occur at deeper levels (cf. Table 1). IC data from the lower part of the upper violet slates are similar to those of the middle violet slates plotting within the middle anchizone ($\Delta°2\theta = 0.3$–0.4; Fig. 2). The change from diagenesis/anchizone transition to the anchizone within the upper violet slates is well developed between Katsidoni and Roussa Ekklisia. The violet slates on top of the Prinias mountain, located between both villages, show high IC values and partly contain kaolinite besides pyrophyllite and paragonite–illite mixed layers. The quartzite-bearing slates, exposed at deeper levels close to Roussa Ekklisia, show Fe-carpholite and lower IC values that reflect the middle anchizone.

The lowest IC values appear in the metasediments which rest unconformably on top of the pre-Alpine basement. In Table 1 these rocks are referred to as Chamezi beds (Metaandesit-Formation of Haude, 1989). The data indicate the anchi-/epizone transition ($\Delta°2\theta = 0.2$–0.3; Fig. 2). In the marble/phyllite interbedding, lower violet slates, and rauhwacke–dolomite–gypsum formation, exposed below the pre-Alpine basement, the IC data indicate the middle to higher anchizone. The same holds for the Kalavros beds and the Plattenkalk rocks below the Kalavros beds. The most frequent mica phase detected in the sequence below the pre-Alpine basement is paragonite.

5.2. Structural evolution, microfabrics and deformation mechanisms

The deformation of the PQU includes several phases depending on the metamorphic grade and the type of lithology (competent or incompetent). It has to be emphasized that, despite intense deformation, the *sedimentary layering*

Table 1
Data of illite crystallinity (IC) and distribution of metamorphic index minerals in the Phyllite–Quartzite unit and in the upper part of the Plattenkalk unit of eastern Crete. Chamezi beds denote the variegated series on top of the pre-Alpine basement. Kalavros beds denote the limy 'flysch' of the Plattenkalk unit. Pg = paragonite, Prl = pyrophyllite, Fcp = Fe-carpholite, Kln = kaolinite

Sample	Locality	Rock type	IC (2θ)	Error (2σ)	Further minerals detected
970422/1-1	Road cut between Epano Episkopi and Ag. Georgios	Upper violet slates	0.430	0.010	Pg, Prl, Pg-illite mixed layer
970425/4-1	Road cut between Skordilo and Kato Kria	"	0.522	0.007	Fcp, Pg, Pg-illite mixed layer
970425/8-1	Road cut between Stavrohori and Koutsouras	"	0.458	0.005	(Pg)
980514/1-3	Pathcut S' Palekastro (metasandstone formation after Haude)	"	0.546	0.013	
980514/1-4	"	"	0.543	0.004	Prl, (Kln), Pg-illite mixed layer
980514/1-6	"	"	0.436	0.004	
980515/1-2	Top of Prinias ('Kramenzelschiefer')	" (top)	0.497	0.007	Prl, Kln, (Pg), Pg-illite mixed layer
980515/2-1	Track at the branch to Xonos, E' of Prinias	" (top)	0.553	0.009	Prl, Pg, Pg-illite mixed layer
980515/4-2	Road cut between Krioneri and Roussa Ekklisia	" (basal)	0.328	0.007	Fcp
980520/3-1	Road cut W' Stavromenos (close to the entrance to the village)	Upper violet slates	0.478	0.024	
980520/7-2	Road cut between Katsidoni and K. Dris, above Sandali	"	0.493	0.020	Fcp
N240649d	Road cut between Paraspori and Achladia	"	0.435	0.012	
N260652	"	"	0.437	0.002	Prl, (Pg), Pg-illite mixed layer
N240649B	Road cut between Paraspori and Achladia	"	0.533	0.008	Pg
970424/3-3	Death valley close to Zagros	"	0.587	0.046	Pg, Pg-illite mixed layer
980520/6-1	Eastern entrance of Sitanos	"	0.394	0.022	Pg, Prl
N240649A	Road cut between Paraspori and Achladia	"	0.502	0.017	
970424/1-2	Eastern entrance of Palekastro	"	0.594	0.005	Prl, Pg-illite mixed layer
N240645G	Paraspori	"	0.446	0.012	Prl, ?Pg, Pg-illite mixed layer
970424/2-1	Between Kelaria and Adravasti	"	0.340	0.034	Prl, Fcp
970424/2-2	"	"	0.326	0.029	Prl, Fcp
990502/1-1	Bay between Toplou and Agio Fotia	"	0.531	0.007	(Prl), ?Pg-illite mixed layer
990502/1-2	Bay between Toplou and Agio Fotia	"	0.479	0.003	?Illite/Pg mixed layer
990502/1-4	Bay between Toplou and Agio Fotia	"	0.439	0.005	Prl
990503/2-3	Between Roussa Ekklisia and Krioneri	"	0.555	0.004	?Illite/Pg mixed layer
990503/3-2	Parking place E of Krioneri	"	0.539	0.023	Prl
220400/1-5	Akr. Tenta, N of Palekastro	Red slate	0.613	0.016	?Illite/Pg mixed layer
230400/1-3	Path cut S' Palekastro ('Metasandstein-Sch.' after Haude)	Upper violet slates	0.637	0.007	(Prl)
250400/1-2	Akr. Tenta	Ankeritic dolomite	0.577	0.091	Prl, ?Pg
981106/1-1	SW margin of Agia Fotia	Upper violet slates	0.492	0.031	Prl, ?Illite/Pg mixed layer
980512/2-1	Track between Chamezi and Linares	Middle violet slates	0.291	0.002	Prl
980520/2-3	Akr. Vamvakia, NW' of the lighthouse	"	0.348	0.008	
N120635	1 km SSE' Skopi (top of the hill)	"	0.347	0.004	
980512/1-1	Road cut between Chamezi and Linares	"	0.299	0.006	Pg
990502/2-4	Road cut E of Vai beach	?Middle violet slates	0.350	0.011	-
980513/2-1	Track S' Linares (below th patch reefs)	Chamezi beds on top of pre-Alpine b.	0.316	0.008	Pg
N120636	1 km SSE' Skopi	"	0.292	0.002	

Table 1 (*continued*)

Sample	Locality	Rock type	IC (2θ)	Error (2σ)	Further minerals detected
970403/1-1	Road cut between Skopi and Chamezi	"	0.245	0.031	
970420/1-3	Between Sitia and Agia Fotia	"	0.221	0.030	
970421/4-2	Erimoupolis	"	0.272	0.033	
970421/4-4	"	"	0.227	0.041	
990502/2-2	Vai beach	?Chamezi beds	0.334	0.009	(Pg)
210400/1-3	S of Vai beach	?Chamezi beds	0.506	0.018	(Prl)
970414/1-6	Minoan yard, below the main thrust	Limy phyllite (phyllite/marble interb.)	0.313	0.002	(Pg)
980518/5-2	Road cut between Sfaka and Tourloti	"	0.301	0.017	Pg
980512/3-1	Road cut E' Paraspori	"	0.326	0.022	Pg
970425/6-1	Road cut between Hrisopigi and Lapithos	"	0.332	0.004	(Pg)
980524/2-1	Sharp bends of the road below Orinon	Limy phyllite below Tropolitza	0.376	0.012	Pg
N290522	Church of Paraspori	Limy phyllite (phyllite/marble interb.)	0.272	0.003	
N290524	500 m N' Paraspori	"	0.345	0.005	(Pg)
S040646B	Minoan yard, between Chamezi and Exo Mouliana	"	0.304	0.007	Pg
S290611	1.25 km E' Exo Mouliana	"	0.270	0.008	
S230531	1 km SE Chamezi	"	0.279	0.002	(Pg)
S280681A	SE of Chamezi	?Limy phyllite	0.275	0.007	
S290612	Road cut between Minoan yard and Chamezi	Limy phyllite	0.312	0.008	Pg
S290683	Exo Mouliana	?Limy phyllite	0.252	0.003	
S2906/OG/1	E' Exo Mouliana	Limy phyllite (phyllite/marble interb.)	0.344	0.012	Pg
N260651	Road cut between Paraspori and Achladia	"	0.305	0.005	?Pg
970415/1-4	Between Chamezi and Exo Mouliana	"	0.359	0.031	Pg
970417/3-1	Between Mirsini and Messa Mouliana	"	0.320	0.002	?Pg
970414/1-4	Between Chamezi and Exo Mouliana	"	0.278	0.047	Pg
970414/1-5	"	"	0.283	0.030	?Pg
970418/2-1	Between Mirsini and Sfaka	"	0.317	0.058	
970418/2-2	"	"	0.285	0.037	
S210663B	1 km E' Exo Mouliana	Lower violet slates	0.328	0.011	Pg
S230670	0.75 km E' Exo Mouliana	"	0.355	0.009	Pg
S210663	1 km E' Exo Mouliana	"	0.434	0.006	Pg
980513/4-1	Path between Leopetra and Linares (above the chapel)	"	0.314	0.007	Pg
N200642	1 km W' Paraspori	"	0.306	0.004	
970504/2-3	Track SW' Kalavros	"	0.374	0.008	Pg
970419/3-3	"	"	0.380	0.001	
S290610	1 km E' Exo Mouliana	"	0.290	0.008	Pg
S180522/1	Road cut E' Exo Mouliana	"	0.357	0.027	Pg
S290610D	Exo Mouliana	"	0.351	0.025	Pg
970415/1-1	Between Chamezi and Exo Mouliana	"	0.296	0.054	?Pg
970415/1-2	"	"	0.302	0.017	?Pg
981107/2-2	E of Kalavros	"	0.387	0.034	Pg
S220668	1 km ESE' Exo Mouliana	Rauhwacke on top of Kalavros beds	0.303	0.007	
970419/3-1	Mochlos beach	Kalavros beds	0.294	0.003	
970504/2-5	"	"	0.302	0.007	
980518/2-2	Road cut between Sfaka and Lastros	"	0.297	0.002	
S040646c	Minoan yard, between Chamezi and Exo Mouliana	"	0.311	0.005	(Pg)

Table 1 (*continued*)

Sample	Locality	Rock type	IC (2θ)	Error (2σ)	Further minerals detected
S130654A	1.25 km E' Exo Mouliana	"	0.317	0.004	Pg
S150658	1 km SSW' Chamezi	"	0.329	0.004	(Pg)
S290603B	Exo Mouliana	"	0.330	0.003	
970504/2-4	Track SW' Kalavros	Kalavros beds (with Mg-Riebeckit)	0.366	0.018	Pg
970416/1-4	Between Chamezi and Exo Mouliana	Kalavros beds	0.275	0.024	
970504/2-2	Track SW' Kalavros	Kalavros beds (with Mg-Riebeckit)	0.237	0.036	
990503/1-2	W part of Leopetra	Plattenkalk limestone	0.237	0.002	–
S310541	Exo Mouliana	"	0.308	0.014	
S290604B	300 m SE' Exo Mouliana	"	0.278	0.005	(Pg)
980518/1-2	Road cut between Sfaka and Lastros	"	0.342	0.005	(Pg)

(S_0) is preserved within all tectonic subunits. This holds particularly for competent rocks such as metasiltstone, metasandstone, metaconglomerate and marble (Figs. 3a and b and 4d). In the metasandstones of the upper violet slates, cross-bedding and ripple marks are well preserved. Moreover, in the uppermost part of the violet slates, horizons with sparitic spheroids ('pseudoooids') represent S_0 fabrics.

5.2.1. D_1 deformation

A first deformation phase (D_1) is rarely documented by E–W-trending isoclinal folds and related S_1 cleavage that is commonly aligned subparallel to S_0 (Fig. 4d). Because of strong and pervasive D_2 deformation, such D_1 folds occur as relicts, particularly within the phyllite–marble interbedding and in the lower violet slates where small layers of quartzite and marble have been folded, partly with vergence to the south. In competent metapsammitic and marble layers the D_1 stage is further documented by extensional veins, which are filled with calcite or quartz, respectively. As the D_1 structures are rare and in most cases overprinted by younger deformation structures, the D_1 kinematics and deformation mechanisms can hardly be assessed.

5.2.2. D_2 deformation

The most pervasive strain was produced during the D_2 deformation that includes both top-to-the-SSE shearing and NNW–SSE coaxial stretching. The orientation of the stretching lineation is depicted in Figs. 1 and 5a. It has to be noted that both coaxial and noncoaxial domains frequently show $L > S$ tectonites and D_2 folds (Fig. 3a). The D_2 folds occur from millimeter to several meter scale and their axes are aligned parallel to the stretching lineation.

Coaxial NNW–SSE stretching is indicated by: (1) viscous, prolate elongation of limestone and pyroclastic pebbles in metaconglomerate on top of the pre-Alpine basement, (2) symmetric boudinage of competent beds like quartzite in pelitic or limy matrix (Fig. 3b), (3) steeply inclined, ENE–WSW striking tension gashes within competent beds and within rigid dolomite and quartzite pebbles of metaconglomerates (Fig. 5b); in the lower part of the upper violet slates and in the middle violet slates these gashes are frequently filled with Fe-carpholite, and (4) symmetric pressure shadows of calcite or quartz fibers behind rigid quartz or clasts (Fig. 4f). In the upper violet slates the S_2 cleavage is frequently developed as pencil cleavage.

Macroscopic and microscopic top-to-the-SSE sense of shear is indicated by SC and shear-band fabrics, which are present in marble–phyllite layers, in retrograde shear zones of the pre-Alpine basement and in the Kalavros beds (Fig. 6e). The D_2 shear zones within micaschist and gneiss of the pre-Alpine basement are some decimeters thick and strikingly dark due to large amounts of retrograde chlorite. Top-to-the-SSE kinematics within these shear zones are further indicated by asymmetric pressure shadows of quartz + phyllosilicate behind quartz clasts. In high-strain domains, the quartz within the pressure shadows shows evidence for strain-induced grain-boundary migration suggesting deformation regime 1 of Hirth and Tullis (1992). The old pre-Alpine quartz grains, however, show less intense Alpine recrystallization. In most cases the pre-Alpine microfabrics are well preserved. If the quartz clasts are embedded in phyllosilicate-rich matrix, they are strongly affected by pressure solution (cf. Schwarz and Stöckhert, 1996).

Within the upper violet slates, D_2 recrystallization of quartz has been observed only in one sample derived from the lower, anchimetamorphic part, where Fe-carpholite exists. In the upper part of the violet slates, where metamorphism straddles the diagenesis/anchizone boundary, recrystallization of quartz is entirely lacking. Microfabrics in quartz consist of undulose extinction, fracturing, deformation lamellae, kink bands, weakly developed subgrains and sutured boundaries due to pressure solution.

The difference in metamorphic grade between the upper violet slates and the units underneath is further reflected by the calcite fabrics, particularly within D_1 calcite veins.

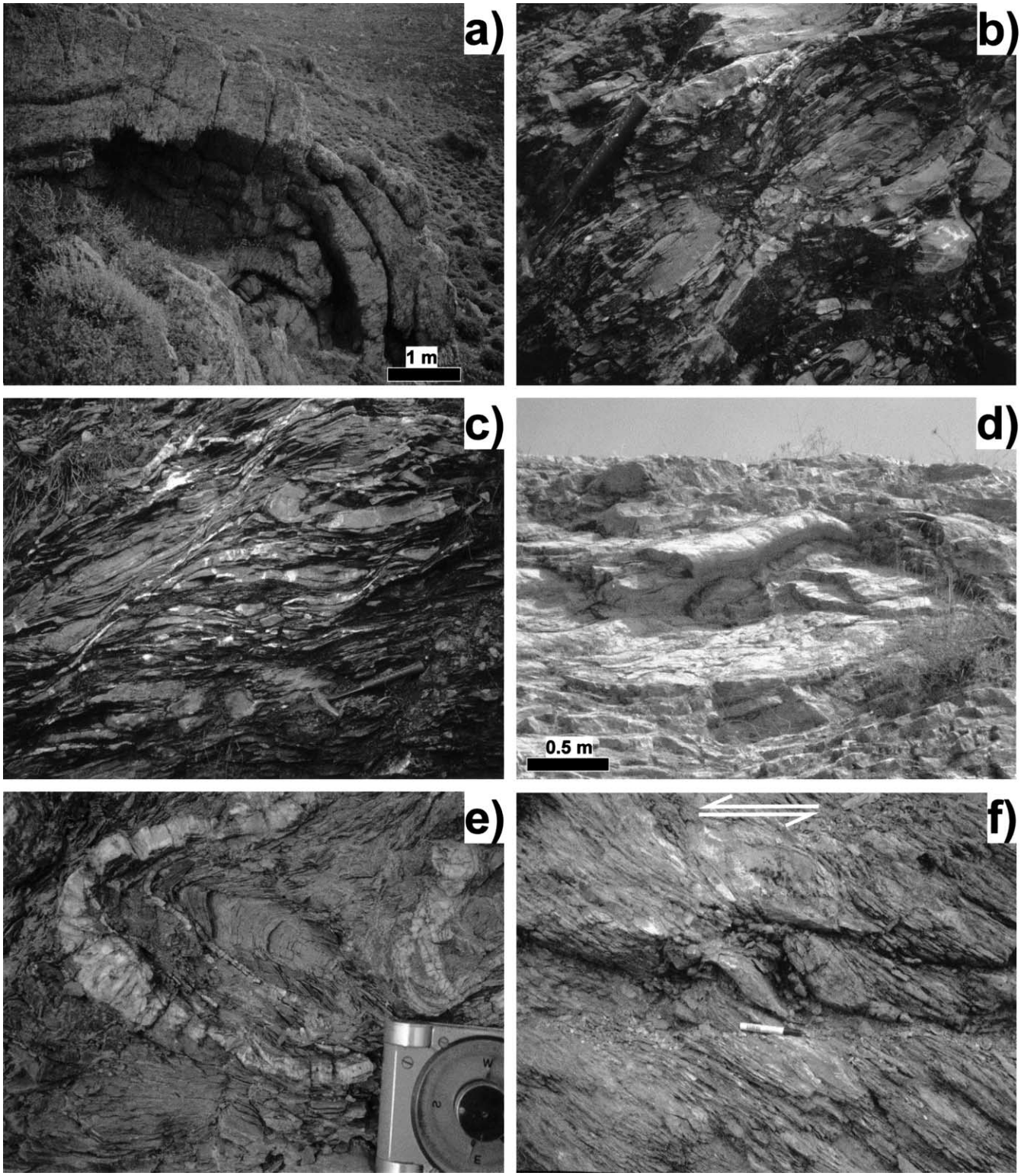

Fig. 3. Characteristic macroscopic deformation structures of the Phyllite–Quartzite unit of eastern Crete. (a) N–S trending open D_2 fold in metaconglomerate with fold axis parallel to the stretching lineation. 1 km NW of Akr. Tenta, NE of Palekastro. (b) Boudinage of metaquartzite layer within weak matrix of limy phyllite and marble of the phyllite–marble interbedding indicates NNW–SSE directed D_2 coaxial stretching. Note that the boudin neck is filled with vein quartz. Road cut W of the Minoan Yard close to Chamezi. (c) Semibrittle N-dipping D_3 normal shear zone in phyllite–marble interbedding. Road cut W of the Minoan Yard close to Chamezi. (d) Open E–W-trending D_4 fold affecting N–S-trending D_2 fold. Escarpment at football ground of Exo Mouliana. (e) E–W-trending D_4 fold affects a quartz–carpholite vein that is aligned subparallel to S_2 within metasiltstone of the lower, anchimetamorphic part of the upper violet slates. Note that the axial-plane cleavage (S_4) is a fracture cleavage. Road cut between K. Dris and Sandali. (f) Duplex in cataclastic D_4 thrust of phyllite–marble interbedding indicates top-to-the-S sense of shear. Path cut between Skopi and Linares.

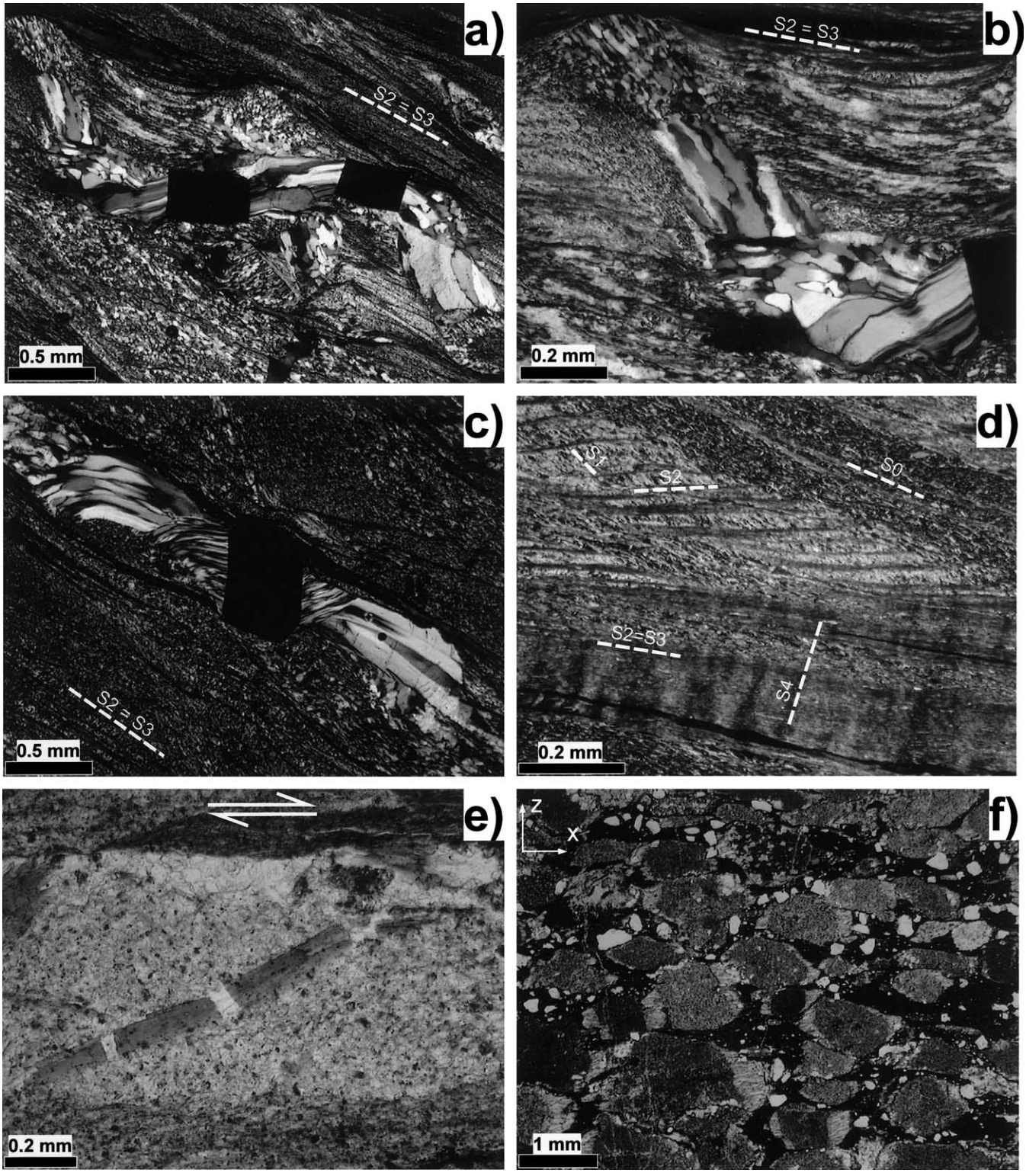

Pre-D_2 vein calcite of the Kalavros beds, of the phyllite–marble interbedding and of the prolate metalimestone-conglomerate, intercalated between metaandesite and Chamezi marble, shows subgrains, broad twin lamellae, which are frequently bent, and sutured grain boundaries that result either from pressure solution or from grain-boundary migration (Fig. 6d). Newly formed recrystallized grains are largely restricted to sutured original grain boundaries. According to the classification of Burkhard (1993) these calcite fabrics are referred to as type III and IV twins that suggest $T >$ ca. 250 °C. Pre-D_2 vein calcite of the uppermost violet slates is also twinned (type II twins

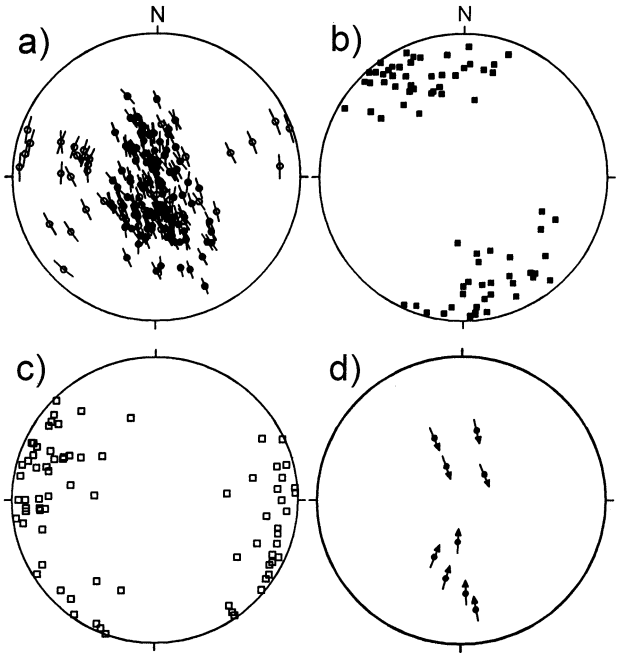

Fig. 5. Structual data plotted in equal-area lower-hemisphere projection. (a) Poles to S_2 planes with related D_2 stretching lineation, plotted after method of Hoeppener (1955). Open circles denote such cases where stretching lineation is parallel to D_2 fold axis. (b) Poles to the planes of mineralized D_2 tension gashes. (c) Direction of D_4 fold axes. (d) Poles to D_3 semibrittle normal shear zones and related movement direction. Arrow shows movement direction of hanging wall.

according to the classification of Burkhard (1993)) and shows evidence for pressure solution, but not for recrystallization.

Of particular interest is the tectonic contact between Kalavros beds and lower violet slates exposed W of Kalavros (the gypsum–rauhwacke–dolomite unit is lacking here). In high-strain domains of sheared impure marble layers, riebeckite prisms grew across D_1 calcite veins (Fig. 6f) and were subsequently rotated towards the stable S position of D_2 mylonites where they suffered fracture boudinage. The boudin necks are filled with calcite (Fig. 4e).

Detailed information about D_2 (and D_3) strain increments and related metamorphic conditions have been obtained from quartz fibers that grew behind rigid pyrite cubes (Fig. 4a–c). These fabrics have been found in metasiltstones, which are intercalated with limy phyllites exposed between Chamezi and Exo Mouliana. The main foliation of these rocks dips 35° to the N. It is strongly controlled by solution–precipitation creep and partly forms the C plane of SC mylonites that result from D_2 top-to-the-SSE and reactivative D_3 top-to-the-N shearing. The reactivation is documented only in those rocks that show a closely spaced interbedding of metapsammitic and metapelitic domains (Fig. 4a–d).

The direction and length of the individual quartz fibers have been measured in thin sections (*XZ*-sections). Examples for complex and less complex fibers are depicted in Figs. 7 and 8, respectively. Most of the fibers are displacement controlled (in the sense of Ramsay and Huber (1983, p. 268)). Their complex growth pattern suggests that the C planes were multiply active and the growth direction of the fibers were largely subparallel to the S planes of the SC mylonite. This holds for both D_2 top-to-the-SSE and reactivative D_3 top-to-the-N shearing (see below). It is obvious from Fig. 4a and c that only the older fibers show trails of fluid inclusions, which are aligned perpendicular to the fiber long axes suggesting a crack-seal mode of fiber growth (cf. Ramsay, 1980). Moreover, Fig. 4a–c also shows that the oldest fibers are recrystallized (bold dashed lines in Fig. 7) and have been affected by progressive shearing and pressure solution along the C planes. The recrystallized fibers grew subparallel to the S planes of the D_2 mylonite suggesting top-to-the-SSE kinematics (sinistral in Fig. 4a and b). The same sense of D_2 shear is indicated by other shear criteria such as displaced D_1 veins and σ-clasts, the latter consisting of deformed and recrystallized early fibers, which are now imbedded within metapelitic matrix. The degree of recrystallization decreases towards younger fiber increments. The oldest D_2 fibers consist of a mosaic of recrystallized, ca. 30 μm large grains in which the shape of the original fibers is partly still visible (Fig. 4b). The width of these fibers is 20–40 μm. Younger D_2 fibers that grew in the same direction are up to 100 μm wide and their walls still show evidence for grain-boundary migration. The same holds for the next fiber generation that, however, grew in a different direction, which is subparallel to the main foliation, i.e. the C

Fig. 4. Photomicrographs of D_1 to D_4 deformation structures. All sections shown are *XZ* sections cut parallel to the stretching lineation and perpendicular to the main foliation. (a) Complex pressure shadows of quartz fibers behind boudinaged pyrite cube in the phyllite–marble interbedding. Crossed polarizers. Road cut at the Minoan Yard close to Chamezi. For further explanation see text and (b). (b) Detail of (a) showing different strain increments portrayed by quartz fibers. Note that the oldest fibers are recrystallized and affected by pressure solution along the main foliation ($S_2 = S_3 = C$ plane of SC mylonite). Their orientation suggests top-to-the-SSE sense of shear during D_2 (sinistral in photograph). Fibers that grew subparallel to $S_2 = S_3$ suggest coaxial D_2 deformation. The youngest thin non-recrystallized fibers indicate reactivative D_3 top-to-the-N shearing (dextral in photograph; for further explanation see text). (c) Quartz fibers behind pyrite cube reflects largely coaxial D_2 NNW–SSE stretching and subsequent reactivative D_3 top-to-the-N normal shearing. Note the crack-seal fabrics in the oldest fibers. Crossed polarizers. Same locality as in (a). (d) Cross-cutting relationships of sedimentary layering (S_0) and different foliations (cleavages) that result from D_1 to D_4 deformation stages. Crossed polarizers. Same locality as in (a). (e) Brittle boudinage of riebeckite along the S plane of a SC marble–mylonite suggests D_2 top-to-the-SSE sense of shear along the contact between Kalavros beds and lower violet slates. C planes are subparallel to long side of photograph. Boudin necks are filled with calcite. Parallel polarizers. Large boulders ca. 1.5 km WSW of Kalavros. (f) 'Pseudoooids' consisting of sparitic calcite and opaque phases within upper part of the upper violet slates, just below the Tripolitza unit. Fibers of calcite (±quartz) in pressure shadows indicate N–S coaxial stretching during D_2. Parallel polarizers. Death valley between Zagros and Kato Zagros.

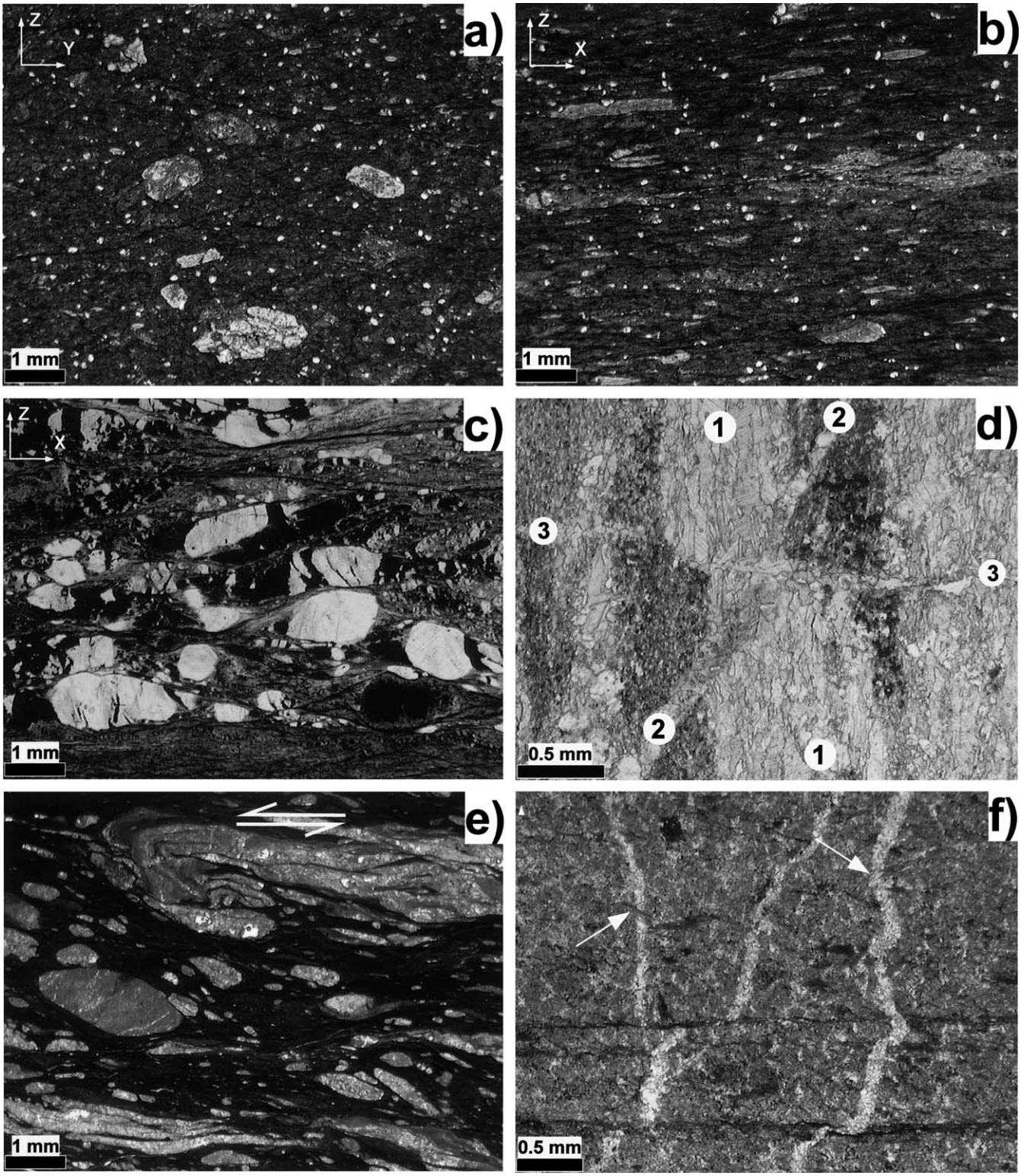

Fig. 6. Photomicrographs of D_1 to D_4 deformation structures, all with parallel polarizers. (a) *YZ* section of a prolate metatuffite. Large elongated clasts consist of chlorite. Small less elongated light clasts are quartz grains. Road cut between Skopi and Chamezi. (b) *XZ* section of the metatuffite shown in (a). (c) *XZ* section of fine-grained prolate conglomerate of upper violet slates. Fracture boudinage of quartz pebbles indicates NNW–SSE stretching during D_2. Boudin necks are filled with opaque phases, largely haematite. Escarpments at Akr. Vamvakia, N of Sitia. (d) Three generations of calcite veins that cut through marble of the phyllite–marble interbedding. Strain-induced grain-boundary migration and type II and III twins (according to the classification of Burkhard (1993)) are restricted to the first vein that pre-dates D_2. Younger post-D_2 veins are largely free from deformation structures. (e) SC mylonite with S-vergent drag fold in impure marble of Kalavros beds indicates top-to-the-SSE sense of D_2 shear. C planes are aligned subparallel to long side of photograph. Road cut between Chamezi and Exo Mouliana. (f) Riebeckite grew across pre-D_2 calcite veins. D_2 thrust contact between Kalavros beds and lower violet slates, ca. 1.5 km WSW of Kalavros.

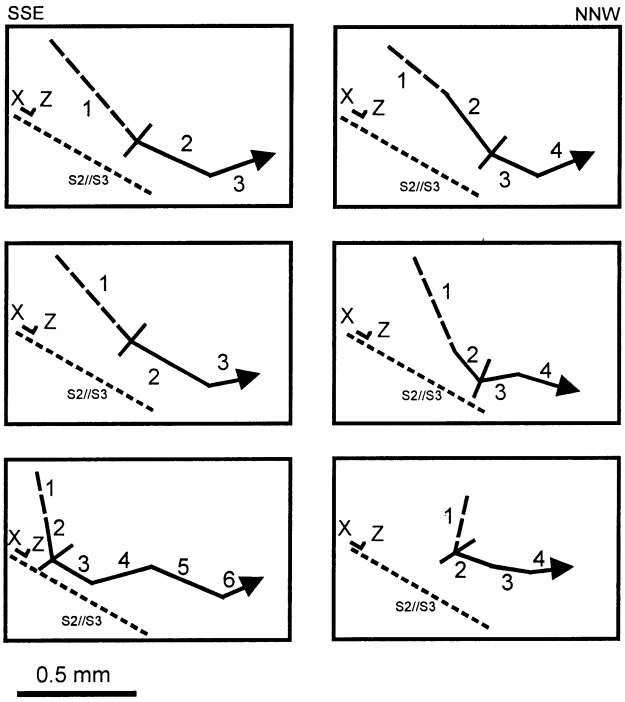

Fig. 7. Line drawing of strain increments in *XZ* sections portrayed by quartz fibers that grew in pressure shadows of pyrite cubes (same rock and locality as in Fig. 4a). Dashed line indicates pervasively recrystallized thin fibers. The oblique line indicates the kinematic transition from D_2 top-to-the-SSE shearing to D_2 coaxial NNW–SSE stretching and to D_3 top-to-the-N reactivative shearing along the $S_2 = S_3$ planes, respectively. For further explanation see text.

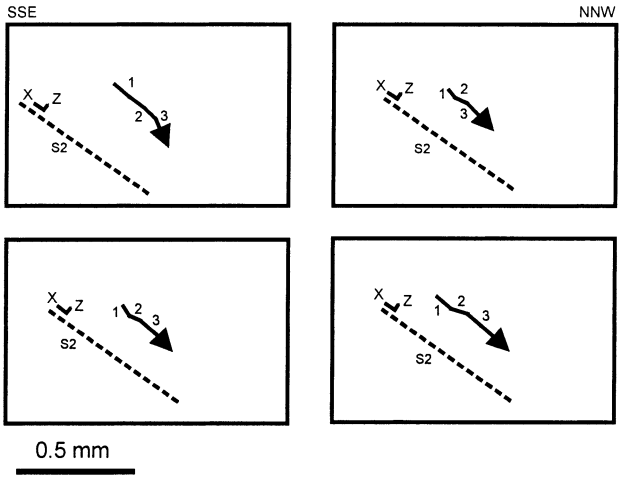

Fig. 8. Line drawing of strain increments in *XZ* sections portrayed by quartz fibers that grew in pressure shadows of pyrite cubes. Same locality as in Fig. 4a but rock is a more competent metaquartzite layer. Fibers record only the older D_2 deformation including top-to-the-SSE shearing and coaxial stretching.

planes, suggesting a phase of coaxial strain. The increasing width of the fibers may reflect progressive burying and related temperature increase during D_2.

5.2.3. D_3 deformation

A new phase of noncoaxial deformation, now with opposite, top-to-the-N sense of shear, led to a second change in the growth direction of the above described quartz fibers that again developed along the S planes of SC mylonites, however, now related to D_3. As the older C planes were reactivated during this deformation phase, they represent both S_2 and S_3 planes. The reactivation of the C planes is also indicated by the finite strain data that will be presented below. Moreover, there are independent shear criteria, such as displaced veins, that prove the top-to-the-N sense of shear during D_3. Similar to the oldest D_2 fibers, the width of the youngest D_3 fibers is again very small, in the range of a few micrometers, suggesting continued uplift and cooling during D_3. Decreased temperatures during D_3 shearing is further indicated by the lack of recrystallization of the fibers and by the fact that chlorite is the only phyllosilicate phase that partly grew together with quartz in the fibers.

Given that the 35° N-dipping foliation of the above-described pyrite-bearing limy phyllite did not significantly rotate during post-D_3 deformation, the D_3 shearing should reflect semibrittle normal movements and thus crustal extension. Evidence for semibrittle normal shearing has further been found at other places, particularly in the marble–phyllite interbedding, where the main foliation (S_2) is frequently displaced by D_3 normal shear zones. However, semibrittle D_3 normal shear zones are entirely lacking within the upper violet slates. It has to be emphasized that—in contrast to the younger D_5 high-angle cataclastic normal faults—the discrete semibrittle D_3 normal shear zones did not lose their cohesion and partly show a foliation (Fig. 3c). Most of these D_3 normal shear zones are dipping moderately or with low angle either to the N or to the S suggesting approximately N–S directed extension (Fig. 5d). The microfabrics of deformed quartz and calcite, which had formed in veins of the phyllite–marble interbedding, confirm the semibrittle character of the D_3 normal shear zones. Calcite shows broad twins, which are bent suggesting $T >$ ca. 200 °C according to Burkhard (1993). Quartz shows deformation lamellae, intense subgrains aligned parallel to the prism planes and local, weak grain-boundary migration. Pervasive recrystallization and formation of new small grains did not occur either in quartz or in calcite. As has been described above, the S_2 foliation was a plane with reduced shear strength that was favorably oriented for D_3 reactivation. This is the reason why many of the S_2 mylonites, particularly those of the pre-Alpine basement, show both top-to-the-SSE and top-to-the-N shear-sense indicators.

5.2.4. D_4 deformation

The main foliation (S_2) and the discrete semibrittle normal shear zones (S_3) were affected by D_4 folding and shearing (Fig. 3d). With respect to kinematics and strain, the D_4 folds are entirely different to the D_2 folds. D_4 folds are classical buckle or even chevron folds where stretching along the fold axes did not occur. The orientation of the

fold axes varies over a wide range, but on average they are trending E–W (Fig. 5c) and frequently show vergence to the S. It is obvious from Fig. 1 that D_4 folds form map-scale structures in the area of the Orno Oros. The Plattenkalk unit crops out in the hinge of a large D_4 anticline. Towards the north the rocks of the PQU are situated in the core of a large D_4 syncline, referred to as Mirsini syncline, because rocks of the Plattenkalk unit are again exposed further to the N at Mochlos, Kalavros and Leopetra. The S_4 axial-plane cleavage of competent beds (including calcite–marble) is a widely spaced fracture cleavage. In anchimetamorphic metapelitic parts, S_4 is also widely spaced and characterized by crenulations and pressure solution. In the phyllite–marble interbedding the hinges of D_4 folds are thickened whereas the limbs are thinned pointing to syn-D_4 material transfer by solution–precipitation creep. Duplex structures together with a well developed P foliation within sub-horizontal cataclastic shear zones (Fig. 3f) indicate top-to-the-S sense of shear, which is consistent with the S vergence of overturned D_4 folds. Clear evidence shows that D_4 folding and related thrusting postdate D_3 semibrittle normal shearing and is present within the pyrite-bearing limy phyllite of the phyllite–marble interbedding described above. Within phyllosilicate rich parts, the $S_2 = S_3$ foliation of these phyllites is slightly crenulated during D_4 folding resulting in a widely spaced gradational S_4 crenulation cleavage (Fig. 4d).

5.2.5. D_5 and D_6 brittle events

The D_4 folds and thrusts are cut by brittle high-angle D_5 normal faults, which are commonly striking E–W. At some places these normal faults have been inverted during subsequent convergence (D_6). Further details on the brittle events will be published elsewhere.

5.3. Finite strain

The finite strain data are listed in Table 2. To visualize both strain magnitude and geometry, the ellipticity of the finite strain ellipse (R_{XZ}) and the Lode's parameter (ν) are depicted in Fig. 2.

In all cases where the R_f/ϕ method has been applied to determine particle strain, the ellipticity of the finite strain ellipse is higher than the maximum ellipticity of the original undeformed particles ($R_S > R_{i(\max)}$). The R_f/ϕ and Fry strain are almost the same in the 'pseudoooid' horizons of the upper violet slates and in cases of relatively fine-grained metaconglomerates that are free from calcite. In cases where fine-grained psammitic rocks like siltstone contain large amounts of calcite (e.g. Kalavros beds), the Fry strain is significantly higher than the R_f/ϕ strain. In some other cases of matrix-supported clastic rocks the R_f/ϕ strain is higher than the Fry strain, which is more difficult to explain, for example by inhomogeneous deformation of the matrix. This is obviously the case in the metatuffites exposed near Chamezi, where chlorite aggregates served as marker grains, which are mechanically weaker than the matrix.

Another rock where the R_f/ϕ strain is considerably higher than the Fry strain needs particular attention. It is the pyrite-bearing limy phyllite from which D_2 top-to-the-SSE and D_3 top-to-the-N shearing has been described above. The Fry strain is based on measurements of the position of the centers of the pyrite cubes. Its value in the XZ section is 2.3. In the same section the R_f/ϕ particle strain, that includes the ellipticity of pyrite + quartz in pressure shadow, is 3.2. As the overall strain is almost plane, simple shear can be assumed during the D_2 top-to-the-SSE and D_3 top-to-the-N shearing. The growth of fiber minerals in pressure shadows has been modeled for simple shear by Etchecopar and Malavieille (1987). They could show that the bulk strain should be the square of the particle strain, the latter including pyrite cube + fiber minerals. Thus, in our case the bulk strain should be $3.2^2 = 10$, a value that is by far not compatible with our data. However, the low Fry strain can be explained by the fact that the reactivation of the D_3 shear planes brought the pyrite grains close to their original position, meaning that the D_2 shear strain was reduced by D_3 retroshear. Thus, the difference between expected and analyzed Fry strain further supports the reactivation concept outlined above.

The shape of the finite strain ellipsoid varies from flattening via plane through prolate (Fig. 2). Flattening fabrics are restricted to very fine-grained samples that include calcite in the matrix (e.g. Kalavros beds). Plane strain is widespread in the upper violet slates, particularly in the 'pseudooolith' horizons, and in some metapsammitic rocks on top of the pre-Alpine basement, which are free from carbonaceous material. Prolate strain has been frequently determined in fine-grained metaconglomerates, metatuffites and metasiltstone, all of which do not include calcite material.

The strain magnitude is reflected either by the ϵ_S value (Table 2) or by the ellipticity of the finite strain ellipse of the XZ section (R_{XZ}; Fig. 2). The highest R_{XZ} values, up to seven, have been found in metaconglomerates that include large amounts of limestone pebbles. These metaconglomerates are part of the variegated series that rests on top of the pre-Alpine basement. Relatively high strain magnitudes are further present in the pyrite-bearing limy phyllites of the marble/phyllite interbedding and in the Kalavros beds.

In the 'pseudoooid' horizon and in a fine-grained metaconglomerate of the upper violet slates it was possible to measure the longitudinal strain along the main stretching direction (e_x) using fiber minerals in pressure shadows of rigid particles. In cases where the strain was largely coaxial and the particle and matrix strain were similar, we could combine the longitudinal strain with the ellipticity of the finite strain ellipsoid in the principal sections for calculating the volumetric strain (ΔV). It has to be emphasized that the error of the volumetric strain, as listed in Table 2, is exclusively controlled by the error of e_x. Either volume gain of up to 150% or volume constancy has been determined for the

'pseudoooliths' (Table 2). Clear volume constancy in one of them is compatible with our cathodoluminescence (CL) data, which show that the calcite of the pseudoooids is similar to that of the fibers of the pressure shadows. The CL color of both is relatively dark. On the other hand, calcite of late extensional veins that cut the pseudoooids and the fibers (Fig. 4f) show light CT color suggesting a different, remote source of calcite solution. The other rock type, where about 100% volume gain has been determined, is a fine-grained metaconglomerate that includes quartz pebbles with fracture boudinage. The fractures are filled with opaque phase that probably consists of hematite. Apart from one sample of 'pseudooolith' that shows flattening strain, the rocks from which volume constancy or volume gain has been determined are characterized by plane or slightly prolate strain.

5.4. Paleopiezometry

The differential stress derived for the D_2 deformation stage is depicted in Tables 3 and 4 and in Fig. 2. Table 3 also includes principal parameters and the mean size and standard deviation of recrystallized grains, all of which are basic prerequisites for the recrystallized-grain-size pieozometer. The error of the calculated differential stresses listed in Table 3 results exclusively from the standard deviation of the grain size. First we will compare the stresses derived from the size of recrystallized grains, calculated according to different calibrations. It is obvious that the data calculated after Twiss (1977, 1980), White (1979) and Etheridge and Wilkie (1981) are quite similar within error (Table 3). The calculations after Mercier et al. (1977) yield lower and the calculations after Koch (1983) and Ord and Christie (1984) yield higher values. The fact that the calibration of Twiss (1977) yields more reliable data compared with the calibration of Koch (1983) has also been emphasized by Gleason and Tullis (1993, 1995).

The lowest differential stresses (ca. 70 MPa) have been determined from the recrystallized quartz fibers of the pyrite-bearing metasiltstone embedded in limy phyllite of the marble–phyllite interbedding. In this paricular case, it is possible that the stress in the pressure shadow does not represent the bulk stress. This is indicated by the other data of the marble–phyllite interbedding calculated after Rowe and Rutter (1990). When regarding the relatively large error bars, they range from 100 to 300 MPa. The highest values have been determined from calcite veins of rigid metavolcanics, where the overall differential stress might have been higher than in the mechanically weaker phyllites and marbles. Differential stresses between ca. 80 and 200 MPa have been found for the Kalavros beds, the metavolcanics and conglomerates on top of the pre-Alpine basement, and in the lower part of the upper violet slate. The highest stress values at ca. 300 MPa have been derived from early calcite veins of the 'pseudooolith' horizon of the upper violet slates. This holds for two samples, which have been taken from entirely different localities (Table 4).

The stress data calculated after Rowe and Rutter (1990) using the amount of twins in calcite per unit length, probably yield less reliable data compared with those of the recrystallized-grain-size piezometer. Two samples have been investigated where both methods could be applied. The data after Rowe and Rutter (1990) are most compatible with the data calculated after Twiss (1977). They are similar within error. In the case of a fine-grained metaconglomerate, the Twiss method was applied to recrystallized fiber quartz of pressure shadows, whereas the Rowe and Rutter (1990) method was applied to calcite of the matrix. The differential stresses derived are 129 $+46/-24$ MPa (after Twiss) and 176 ± 38 MPa (after Rowe and Rutter). The slightly lower value after Twiss may result from the fact that the differential stress was lower in the pressure shadows than in the matrix.

In the second case of a calcite–quartz vein of a metaconglomerate we have derived 99 $+43/-21$ MPa (after Twiss) and 164 ± 67 MPa (after Rowe and Rutter). Although the data are similar within error, when regarding the paleopiezometric data in general we got the impression that the calcite-twin method yields higher stress values than the recrystallized-grain-size piezometer of Twiss.

6. Discussion

6.1. Jumps in metamorphic grade and their influence on rheology

First of all we will compare the IC data, microfabrics of quartz and calcite, differential stress, and finite strain along the tectonostratigraphic sequence of the PQU and the uppermost Plattenkalk unit (Fig. 2). The highest metamorphic grade (temperature) has been determined for the Chamezi beds on top of the pre-Alpine basement. Here the anchi-/epizone transition is indicated by: (1) relatively low $\Delta^\circ 2\theta$ values of illite at ca. 0.25; (2) the presence of pyrophyllite, paragonite and Fe-carpholite, but absence of kaolinite and paragonite–illite mixed layers; (3) D_2 recrystallization of quartz and calcite; (4) type III and type IV calcite twins (according to the classification of Burkhard (1993)); (5) moderate differential stresses during D_2 deformation ranging from ca. 80 to 200 MPa; and (6) pervasive D_2 deformation of different rock types, including metaconglomerates and metavolcanics, associated with maximum finite strains at $R_{XZ} = 6–7$; similar high strain magnitudes have been determined in the PQU of central Crete (Fassoulas et al., 1994). Thus, the relatively low $\Delta^\circ 2\theta$ values of illite cannot be attributed to detrital micas. They result from elevated temperatures that supported recrystallization-accommodated dislocation creep of quartz and calcite. Apart from solution–precipitation creep in phyllosilicate-rich rocks, this thermally activated deformation

Table 2
Strain data derived from rocks of the Phyllite–Quartzite unit and the Kalavros beds

Sample no.	Locality	Rock type	Method[a]	R_{XZ}	R_{YZ}	R_{XY}	k-value (Flinn diagr.)	ν (Hsu diagr.)	ϵ_s (Hsu diagr.)	n[b]	$1+e_x$	$\pm 1\sigma$	$(1+e_x)/(1+e_y)$	$(1+e_z)$	n[c]	$\Delta V_{(min)}$ [%]	ΔV [%]	$\Delta V_{(max)}$ [%]
970402/1-2	Akr. Vamvakia, N' Sitia	Fine grained metaconglomerate	nF	1.8	1.3	1.4	1.3	−0.1	1.5	259 + 437								
"	"	"	R	1.7	1.2	1.4	2.1	−0.3	1.5	259 + 437	1.68	0.05	1.2	1.0	40 80	97		115
970403/1-1a	Between Skopi and Chamezi	Metatuffite	F	2.4	1.3	1.8	2.8	−0.4	1.9	266 + 398								
"	"	"	R	3.6	1.6	2.3	2.1	−0.3	2.6	46 + 53								
970414/1-4	Between Chamezi and Exo Mouliana	Limy phllite with pyrite cubes	F	2.3	1.5	1.5	1.1	−0.0	1.8	137 + 498								
"	"	"	R	3.2	1.4	2.3	3.2	−0.4	2.4	137 + 498								
970414/1-5	Between Chamezi and Exo Mouliana	Metasiltstone within limy phyllite	F	1.8	1.2	1.5	2.5	−0.4	1.5	143 + 202								
970416/1-4	between Chamezi and Exo Mouliana	Kalavros beds (limy metasiltstone)	nF	2.7	2.4	1.1	0.1	0.8	2.2	343 + 431								
"	"	"	R	2.1	2.1	1.0	0.0	1.0	1.8	343 + 431								
970416/2-1	W' Messa Mouliana	Limy metasiltstone	F	1.8	1.5	1.2	0.4	0.4	1.5	205 + 277								
970420/1-2	Between Sitia and Agia Fotia	Fine grained metaconglomerate	nF	2.0	1.4	1.4	1.1	−0.0	1.6	240 + 317								
"	"	"	R	1.8	1.4	1.3	0.7	0.1	1.5	240 + 317								
970420/1-3	Between Sitia and Agia Fotia	Fine grained metaconglomerate	R	3.2	1.8	1.8	1.0	0.0	2.4	204 + 267								
970424/2-1	Between Kelaria and Adravasti	Metasiltstone	F	1.5	1	1.5	∞	−1.0	1.4	267 + 287								
970401/2	500 m N' Skopi	Metalimestoneconglomerate	R	6.4	2.2	2.9	1.6	−0.2	4.3	103 + 105								
970403/1	Between Skopi and Chamezi	Metalimestoneconglomerate	R	5.2	2.1	2.5	1.3	−0.1	3.5	266 + 398								
970420/2-3	Roussa Ekklisia	Metasiltstone in upper violet schists	F	1.4	1.4	1.0	0.0	1.0	1.3	403 + 504								
"	"	"	R	2.2	2.2	1.0	0.0	1.0	1.9	190 + 103								
970416/1-2	Between Chamezi and Exo Mouliana	Limy phyllite	R	3.9	3.0	1.3	0.2	0.6	2.9	96 + 57								
970424/3-2	Death Valley close to Zagros	Red 'oolith' in upper violet slates	nF	1.9	1.4	1.4	0.9	0.0	1.6	303 + 345								
"	"	"	R	1.8	1.3	1.4	1.3	−0.1	1.5	303 + 345	1.37	0.03	1.0	0.8	50 −3	3		10
980515/4-6	Between Krioneri and Roussa Ekklisia	Red 'oolith' in upper violet slates	nF	1.8	1.7	1.1	0.1	0.8	1.6	348 +358								
980515/4-6	"	"	R	1.7	1.5	1.1	0.3	0.5	1.5	348 +358	1.70	0.05	1.5	1.0	53 131	155		181
980514/2-1	S' Palekastro (S' Agathia)	Red 'oolith' in upper violet slates	R	1.8	1.2	1.5	2.5	−0.4	1.5	114 + 153	1.70	0.10	1.1	0.9	33 50	82		118
980514/2-1	"	"	nF	1.8	1.3	1.4	1.3	−0.1	1.5	114 + 153								
990503/2-2	Between Krioneri and Roussa Ekklisia	Red 'oolith' in upper violet slates	R	1.7	1.3	1.3	1.0	−0.0	1.4	156 + 173	1.40	0.03	1.1	0.8	34 15	23		33
S10a	1.2 km E' Exo Mouliana	Lower violet slates	F	1.4	1.4	1.0	0.1	0.8	1.3	223 + 160								
"	"	"	nF	1.8	1.7	1.1	0.1	0.8	1.6	223 + 160								
"	"	"	R	1.6	1.2	1.3	1.3	−0.1	1.4	223 + 160								
S23	600 m SSW' Exo Mouliana	Lower violet slates	nF	1.6	1.5	1.0	0.1	0.8	1.4	245 + 206								
"	"	"	R	1.8	1.2	1.5	2.9	−0.4	1.5	245 + 206								
S54b	1.3 km E' Exo Mouliana	Kalavros beds	nF	1.4	1.1	1.3	2.7	−0.4	1.3	254 + 268								
"	"	"	R	1.3	1.2	1.1	0.4	0.4	1.2	254 + 268								
S62	1.4 km WNW' Chamezi	Metasandstone of Chamezi beds	nF	1.6	1.3	1.3	1.1	−0.0	1.4	250 + 194								
"	"	"	R	1.2	1.1	1.1	2.0	−0.3	1.1	250 + 194								
S65	1 km ESE' Exo Mouliana	Metatuff below lower violet slates	nF	2.1	1.7	1.3	0.4	0.4	1.7	79 + 104								
"	"	"	R	2.5	1.3	2.0	3.8	−0.5	2.0	79 + 104								

Table 2 (*continued*)

Sample no.	Locality	Rock type	Method[a]	R_{XZ}	R_{YZ}	R_{XY}	k-value (Flinn diagr.)	ν (Hsu diagr.)	ϵ_s (Hsu diagr.)	n[b]	$1 + e_x \pm 1\sigma$	$(1 + e_x)$	$1 + e_y$	$1 + e_z$	n[c]	$\Delta V_{(min)}$ [%]	ΔV [%]	$\Delta V_{(max)}$ [%]
S84c	750 m ENE' Chamezi	Metatuff in Chamezi beds	nF	1.4	1.1	1.2	2.1	−0.3	1.2	250 + 262								
"	"	"	R	1.4	1.2	1.1	0.6	0.3	1.2	250 + 262								
980515/1-1	Top of Prinias	Metasandston in upper violet slates	nF	1.4	1.2	1.2	1.1	−0.1	1.2	358 + 332								
"	"	"	R	1.2	1.1	1.1	0.9	0.0	1.1	358 + 332								
980512/2-b	Between OTE and Linares	Metalimestoneconglomerate	nF	2.4	2.4	1.0	0.0	1.0	2.0	122 + 142								
"	"	"	R	1.9	1.7	1.1	0.1	0.7	1.6	122 + 142								
S130653	1.4 km E' Exo Mouliana	Kalavros beds	nF	2.1	1.5	1.4	0.7	0.1	1.7	251 + 517								
S230673a	1 km E' Exo Mouliana	Kalavros beds	nF	2.2	2.1	1.1	0.1	0.8	1.8	193 + 276								
"	"	"	R	2.0	1.5	1.3	0.6	0.2	1.6	194 + 276								
S230673b	"	"	nF	1.8	1.4	1.2	0.5	0.3	1.5	242 + 316								
"	"	"	R	1.6	1.5	1.0	−0.1	1.2	1.4	242 + 316								
N120635c		Middle violet slates	nF	1.8	1.2	1.5	2.0	−0.3	1.5	483 + 351								
"	"	"	R	1.7	1.4	1.2	0.6	0.2	1.5	483 + 351								
970414/1-7	Between Chamezi and Exo Mouliana	Limy phyllite	nF	2.8	2.3	1.2	0.2	0.6	2.2	137 + 117								
"	"	"	R	2.7	2.3	1.2	0.1	0.7	2.2	137 + 117								
970421/4-1	Erimoupolis beach	Limy metasiltstone	F	2.6	1.2	2.2	5.8	−0.6	2.1	135 + 168								
970421/4-1	"	"	R	1.6	1.5	1.1	0.1	0.7	1.4	403 + 462								

[a] R = R_f/ϕ, F = Fry, nF = norm. Fry.

[b] Number of data used to calculate finite strain with R_f/ϕ and Fry method.

[c] Number of data used to calculate longitudinal strain $(1 + e_x)$.

Table 3
Differential stresses related to D_2 deformation derived by using different calibrations, which are based on the grain size of recrystallized quartz grains. Note that the calculated error of stresses results only from the standard deviation in grain size. For locality and rock type of investigated samples see Table 4

Sample	n	Grain size [μm]	Differencial stress [MPa]						
			Twiss (1977, 1980)	Mercier et al. (1977)	White (1979)	Etheridge and Wilkie (1981)	Koch (1983)	Ord and Christie (1984)	
			14500	4070	12900	14200	490	1780	b [μm MPa^{-r}]
			− 1.47	− 1.4	− 1.43	− 1.47	− 0.59	− 0.9	r
970414/1-4	113	30±9	67 +18/−11	33 +10/−6	69 +20/−12	66 +18/−11	114 +95/−41	93 +45/−24	
970421/4-3	83	11±4	129 +45/−24	67 +25/−13	137 +50/−26	128 +45/−24	587 +662/−238	273 +175/−79	
970401/2-2	260	17±7	99 +43/−21	50 +23/−11	103 +46/−22	97 +42/−20	298 +434/−132	176 +141/−56	
970413/1-1	169	9±3	156 +47/−27	81 +26/−15	165 +52/−29	153 +46/−27	927 +864/−349	370 +199/−99	
970423/2-1	157	16±6	105 +46/−22	53 +25/−12	110 +50/−24	103 +46/−22	345 +515/−154	193 +158/−62	
970423/2-2	139	11±4	133 +48/−25	68 +26/−14	140 +52/−27	131 +47/−25	623 +717/−255	285 +186/−83	

Table 4
Differential stresses related to D_2 deformation derived by using the twin-in-calcite method (Rowe and Rutter, 1990) and the recrystallized grain-size piezometer of Twiss (1977, 1980). n = number of grains considered

Sample	Locality	Rock type	Method	n	Stress difference [MPa]	Error [MPa]		Comments
						+	−	
970401/2-1	Road cut 500 m NE' Skopi	Calcite in prolate metalimestoneconglomerate	Rowe and Rutter (1990)	26	137	51	51	
970401/2-2	"	Twiss (1977, 1980)	Twiss (1977, 1980)	260	99	43	21	Qtz in vein with calcite
970401/2-2	"	"	Rowe and Rutter (1990)	72	164	67	67	"
970413/1-1	Road cut SW' Chamezi	Twiss (1977, 1980)	Twiss (1977, 1980)	169	156	47	27	Recrystallized quartz clast
970414/1-2	Road cut between Chamezi and Exo Mouliana	Vein calcite in marble	Rowe and Rutter (1990)	100	215	40	40	Vein Qtz starts to recrystallize
970414/1-4	Road cut W of Minoan yard	Metasiltstone layer in limy phyllite	Twiss (1977, 1980)	113	67	18	11	Qtz in pressure shadow of pyrite
970415/1-3	Road cut between Chamezi and Exo Mouliana	Metavolcanic with calcite vein	Rowe and Rutter (1990)	50	224	52	52	Calcite vein with recrystallization along twin lamellae
970416/1-4	Road cut W of Minoan yard	Marble of Kalavros beds	Rowe and Rutter (1990)	50	121	53	53	Marble
970416/1-5	Road cut between Chamezi and Exo Mouliana	Kalavraos beds	Rowe and Rutter (1990)	73	138	48	48	SC mylonite in Kalavros beds
970418/2-1	Road cut between Mirsini and Tourloti	Greenschist with calcite vein	Rowe and Rutter (1990)	25	263	30	30	Calcite vein in metabasite

Table 4 (*continued*)

Sample	Locality	Rock type	Method	*n*	Stress difference [MPa]	Error [MPa]		Comments
						+	−	
970420/1-4	Beach between Sitia and Agia Fotia	Vein calcite in limestone conglomerate	Rowe and Rutter (1990)	24	150	44	44	
970420/1-5	Peninsula between Sitia and Agia Fotia	Limestoneconglomerate	Rowe and Rutter (1990)	50	142	34	34	Qtz starts to recrystallize
970420/1-6	Beach between Sitia and Agia Fotia	Limestoneconglomerate	Rowe and Rutter (1990)	24	159	62	62	
970421/4-3	Beach at Erimoupolis	Fine grained metaconglomerate	Twiss (1977, 1980)	83	129	45	24	Qtz in pressure shadow of old Qtz grains
970421/4-3	"	"	Rowe and Rutter (1990)	44	176	38	38	Calcite in matrix of conglomerate
970423/2-1	Road cut between K.Dris and Sandali	Upper violet slates (Qtz + Fcp vein)	Twiss (1977, 1980)	157	105	46	22	Partly recrystallization of Qtz in Qtz–Fcp vein
970423/2-2	Road cut between K.Dris and Sandali	"	Twiss (1977, 1980)	139	133	48	25	Partly recrystallization of Qtz in Qtz–Fcp vein
970424/3-2	Deadt valley at Zagros	Upper violet slates ('Metaooid')	Rowe and Rutter (1990)	30	308	23	23	Old calcite vein in 'Metaooid'
970504/2-2	West of Kalavros, at the beach	Shear zone between Kalavros beds and violet slates	Rowe and Rutter (1990)	43	111	78	78	Calcite vein with Mg riebeckit
980513/1-1(xz)	Track between Linares and Hamezi	Calcite mylonite of Chamezi beds	Rowe and Rutter (1990)	50	157	29	29	
980513/1-1(yz)	"	"	Rowe and Rutter (1990)	25	171	33	33	
980513/3-1	Track between Linares and Hamezi (at the chapel)	Limy phyllite	Rowe and Rutter (1990)	18	223	70	70	
980513/3-1	"	"	Twiss (1977) an Calcit	153	91	31	17	
980518/2-1	Between Sfaka and Lastros	Vein calcite in Kalavros beds	Rowe and Rutter (1990)	56	151	50	50	
980514/2-1	Path S' Palekastro, S' Agathia	Upper violet slates ('Metaooid')	Rowe and Rutter (1990)	50	160	27	27	Coarse grained calcite in center of 'ooids'
980518/5-1	Road cut between Tourloti and Sfaka	Limy phyllite	Rowe and Rutter (1990)	31	179	33	33	
970401/2-4	Quarry at Hamezi	Chamezi marble	Rowe and Rutter (1990)	50	168	22	22	
981107/2-3	Track below and east of Kalavros	Lower violet slates	Rowe and Rutter (1990)	30	264	24	24	Calcite vein in marlbe
970417/1-1	Western entrance of Messa Mouliana	Limy phyllite, folded marble	Rowe and Rutter (1990)	50	132	25	25	Calcite vein is partly recrystallized

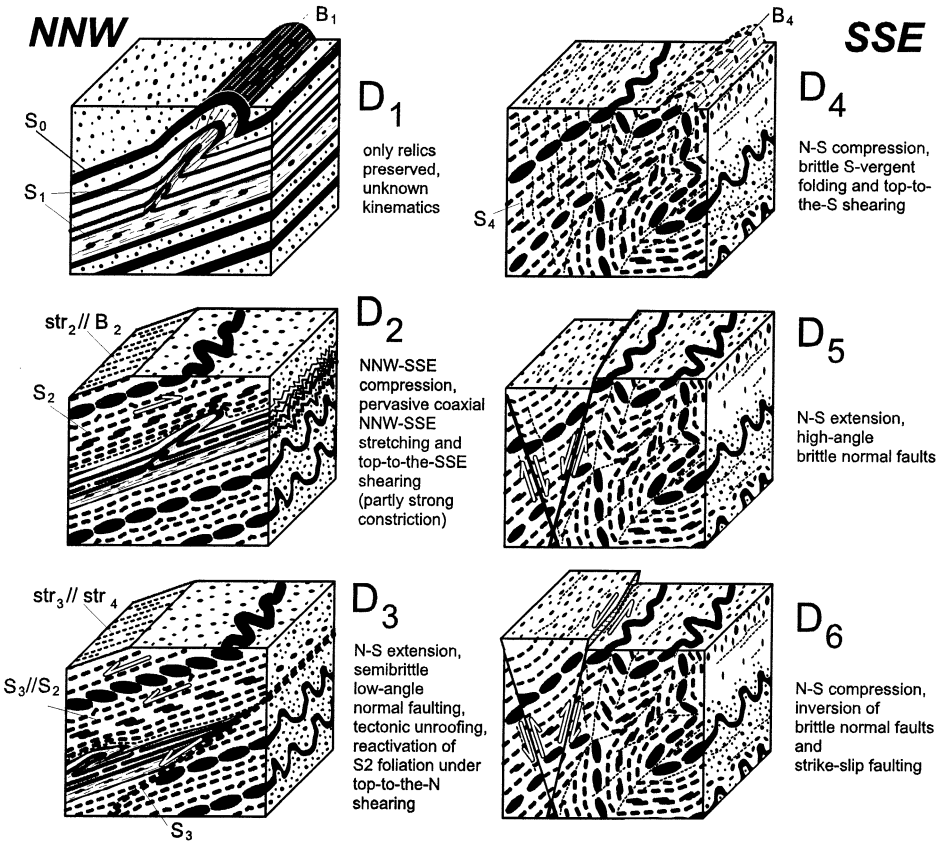

Fig. 9. Deformation stages observed in the rocks of the PQU of eastern Crete. Note that semibrittle normal shearing (D_3) does not occur in the upper part of the upper violet slates where metamorphism is straddling the diagenesis–anchizone transition. For further explanation see text.

mechanism led to rheological softening and related high strains that could develop at moderate differential stresses. The fact that recrystallization of quartz is also present in D_2 shear zones of the pre-Alpine basement suggests that similar metamorphic conditions like those of the Chamezi beds were present in the basement. This assumption is compatible with the temperature interval derived by Franz (1992) for the Alpine shearing along the retrograde shear zones of the basement ($T = 250$–310 °C at $P = 450$–600 MPa).

The differential stresses at the anchi-/epizone transition have been determined with both the recrystallized grain-size and the calcite-twin piezometer. Thus, although the stress data imply relatively large errors and uncertainties, in this case the range of stresses (80–200 MPa) should be reliable to some extent. If we assume a metamorphic temperature of ca. 300 °C for the anchi-/epizone transition (see above) and apply the deformation mechanism maps derived for quartz and calcite by Rutter (1976), with an average grain-size of 100 μm (which is common in the siliciclastic rocks and in the matrix of conglomerates investigated), we are close to the triple junction between dislocation creep, dislocation glide and solution creep. This position is consistent with the microfabrics observed. Moreover, the data of the deformation mechanism maps further suggest that related strain rates were relatively fast $>10^{-12}\,s^{-1}$. Thus, the finite D_2-strain obtained should have formed at periods much less than 1 my. Given the derived stresses of 80–200 MPa have driven only dislocation creep of wet quartz, without involvement of solution–precipitation creep, the resulting strain rates differ considerably depending on the experimental calibration. If we consider the calibrations of Jaoul et al. (1984), Kronenberg and Tullis (1984), Paterson and Luan (1990), and Gleason and Tullis (1995), the differential stresses of 200 MPa at $T = 300$ °C yield strain rates ranging from 8.4×10^{-16} to $9.3 \times 10^{-12}\,s^{-1}$. Differential stresses of 80 MPa result in strain rates between 2.1×10^{-17} and $8.6 \times 10^{-13}\,s^{-1}$. The lowest values have been obtained using the calibrations of Paterson and Luan (1990, line 2) and Gleason and Tullis (1995). They result in unrealistic deformation periods in excess of 10 my.

High strain rates and high differential stresses are not compatible with rheological data derived for the PQU of western Crete, where peak metamorphic temperatures have been determined at ca. 400 °C for a depth of ca. 30 km (see above). In western Crete the differential stresses in phyllites and quartzites should have remained below ca. 15 and ca. 60 MPa, respectively (Schwarz and Stöckhert, 1996; Stöckhert et al., 1999).

There is no doubt about a break in metamorphism within the upper violet slates as is indicated by a wealth of different data, particularly by IC values and by the distribution of metamorphic index minerals. The fact that the upper part

of these violet slates is straddling the diagenesis–anchizone transition is supported by: (1) high $\Delta^{\circ}2\theta$ values >0.4 of those samples which are free from peak-disturbing paragonite–illite mixed layers; (2) the coexistence of kaolinite and pyrophyllite (paragonite); (3) the lack of Fe-carpholite; (4) the presence of paragonite–illite mixed layers; (5) the lack of recrystallization of quartz and calcite; (6) type II calcite twins, even in high-strain domains (according to the classification of Burkhard (1993)); (7) high differential stresses of up to ca. 300 MPa; and (8) low finite strain ($R_{XZ} < 2$) even in calcite-rich rocks. The low metamorphic grade also explains why the detrital white micas of the upper violet slates of Roussa Ekklisia do not yield a plateau age. Dallmeyer and Takasu (1992) have shown that the Ar–Ar system of slate/phyllite appear to be completely rejuvenated under metamorphic conditions appropriate for the transition from the middle to upper anchizone.

Given that the anchi-/epizone and the diagenesis/anchizone transition occur at $T =$ ca. 300 and ca. 235 °C, respectively (see above), the difference in metamorphic peak temperature between the upper part of the upper violet slates and the Chamezi beds is ca. 60 °C. If the geothermal gradient of both tectonic subunits was similarly low during subduction-related metamorphism (ca. 15 °C km^{-1}), the above temperature interval would result in a difference of burying of ca. 4 km.

The remaining rocks of the PQU show metamorphic conditions of the anchizone, which is also compatible with the microfabrics, strain and stress data. The same holds for the Kalavros beds and the Plattenkalk rocks. Soujon and Jacobshagen (1997) determined similar IC data (middle anchizone) for the Plattenkalk rocks of the Orno Oros and Mirabello peninsula.

6.2. Deformation stages related to subduction/collision and exhumation

The difference in metamorphic grade between the upper violet slates and the rocks underneath also explains the difference in the number of deformation stages. Fig. 9 shows the deformation stages derived from the phyllite–marble interbedding below the pre-Alpine basement. A similar sequence of Alpine deformation holds for those rocks for which at least anchimetamorphic conditions have been determined.

The most important deformation event with maximum strain magnitudes is D_2. In all rocks investigated D_2 was related to intense NNW–SSE stretching. There is a clear strain partitioning during D_2 as is indicated by the coaxial and non-coaxial domains. The fact that calcite and quartz of the anchimetamorphic rocks recrystallized during D_2 and that the D_2 stretching lineation is portrayed by high-pressure/low-temperature metamorphic minerals like Fe-carpholite and blue amphibole suggests D_2 to be related to northward subduction and accretion of the microcontinent. This northward subduction concerns continental fragments consisting of the Plattenkalk unit (including the Kalavros beds) and the pre-Alpine basement and its Carboniferous to Triassic cover of the PQU. Northward subduction is also consistent with D_2 top-to-the-SSE sense of shear that led to thrusting and stacking of older (or higher metamorphic) rocks on top of younger (or lower metamorphic) rocks. The pre-Alpine basement behaved relatively rigidly during subduction as is indicated by the discrete, retrograde D_2 shear zones that cut through it. During D_2 top-to-the-SSE shearing, the basement and its Triassic cover have been thrust on top of the Carboniferous to Triassic marble–phyllite interbedding that also should belong to the cover sequence of the basement. Similar thrust contacts along which older rocks have been thrust over younger rocks occur at deeper structural levels (phyllite–marble interbedding on top of Permian lower violet slates, Permian lower violet slates on top of Triassic metadolomite–metarauhwacke member, Triassic metadolomite–metarauhwacke member on top of Paleogene Kalavros beds).

The crack-seal fabrics in the oldest D_2 quartz fibers behind pyrite cubes of the marble–phyllite interbedding suggest a cyclic increase and decrease of the differential stress, related to fluctuations in pore fluid pressure and resulting in unstable, probably seismic movements during D_2 ('seismic pumping'; sensu Sibson et al., 1975; see also Ramsay and Huber, 1987, p. 574). Evidence for intense fluid activity and solution–precipitation creep is further indicated by the observation that even the old quartz fibers were partly removed by pressure solution. Thus, quartz was multiply dissolved and precipitated pointing to fluid-controlled 'quartz-recycling' under progressive shearing. Apart from pressure solution, the quartz fibers underwent dislocation creep by bulging recrystallization. We suppose that the stronger recrystallization of the oldest small quartz fibers is largely related to the fact that these have a higher surface energy and are probably more strongly deformed by dislocation glide than the broader younger fibers, which also show strain-induced grain-boundary migration and partly reflect coaxial stretching. According to Ramsay and Huber (1987, p. 577), the fibers should become unstable at $T >$ ca. 350 °C. The increase in width of D_2 quartz fibers towards younger increments is attributed to increasing temperatures due to progressive burying. The latter may have caused the switch from non-coaxial to coaxial deformation because of enhanced slab-pull forces at deeper structural levels (see below). Evidence for post-peakmetamorphic D_2 deformation, on the other hand, is present at the thrust contact between Kalavros beds and lower violet slates. Given that the blue amphiboles in the D_2 top-to-the-SSE shear zones of this contact reflect the metamorphic peak, the latter should have occurred prior to D_2. This conclusion is compatible with results of Franz (1992).

The fact that in coaxial and non-coaxial domains the D_2 stretching lineation is aligned parallel to D_2 fold axes, and cross-cuttings of stretching lineation and fold axes are lacking, suggests an additional compressional stress parallel

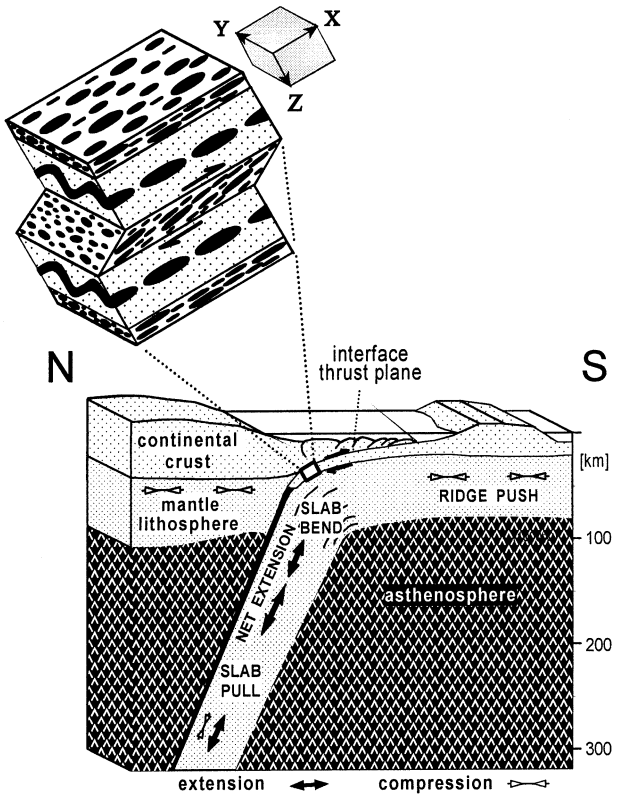

Fig. 10. Kinematic model explaining prolate fabrics and simultaneous formation of D_2 folds and boudins under bulk apparent constrictional strain in subduction/collision environment (modified after Zulauf, 1997, and references therein). Constriction is caused by additional compression parallel to the strike of the downgoing slab. Slab-pull forces led to enhanced coaxial dip-parallel D_2 stretching at deeper levels, while shear stresses along the interface thrust plane led to non-coaxial top-to-the-SSE sense of D_2 shear at the base of the accretionary prism. For further explanation see text.

to the strike of the subduction zone and thus parallel to the *Y*-axis of the finite strain ellipsoid (Fig. 10). Dip-parallel stretching and simultaneous strike-parallel compression can also explain the prolate fabrics that occur more frequently than in central Crete (cf. Fassoulas et al., 1994). As prolate D_2 fabrics are very common in the anchi-metamorphic parts, but are almost lacking in the upper violet slates, which straddle the diagenesis/anchizone transition, we assume that enhanced slab-pull forces at deeper subduction levels additionally supported the formation of prolate fabrics (cf. Zulauf, 1997).

As in fine-grained calcite-rich clastic rocks the Fry strain is significantly higher than the R_f/ϕ strain, solution–precipitation creep may have led to volume loss, the latter pretending D_2 flattening fabrics (cf. Ramsay and Wood, 1973). A similar conclusion has been drawn from the strain data of central Crete (Fassoulas et al., 1994). Volume constancy or even volume gain, on the other hand, is common in the less metamorphic upper violet slates. The difference in strain magnitude between the almost unmetamorphic uppermost violet slates and the anchimetamorphic rocks underneath is similar to the situation of the Peloponnesus. Here the strain in the Tyros beds, which might be an equivalent of the upper violet slates, is much less ($R_{XZ} < 2$) than that of the rest of the PQU ($R_{XZ} > 3$; Xypolias and Doutsos, 2000).

The D_3 extensional stage is documented not only by N- and S-dipping foliated semibrittle normal shear zones, but also by the youngest quartz fibers behind pyrite cubes that reflect reactivative top-to-the-N shearing along the S_2 foliation, probably due to N–S extension. As these fibers are free from recrystallization, the D_3 movements should have occurred either under lower differential stress (strain rate) or under lower temperatures compared with those of D_2. According to the deformation mechanism maps for quartz and for calcite (Rutter, 1976), both shifts should have led to a change from dislocation to dissolution creep. We suppose that a decrease in temperature as well as in differential stress and strain rates have suppressed dislocation creep of quartz. Decreasing temperatures are also indicated by the lack of syn- or post-D_3 metamorphic index minerals such as Fe-carpholite. Thus, D_3 can probably be attributed to the retrograde path of the metamorphic loop. Given that isothermal decompression from ca. 500 to ca. 200 MPa, derived by Franz (1992) for the Alpine shearing of the pre-Alpine basement, also holds for the phyllite–marble interbedding underneath, the D_3 shearing should have occurred at relatively high structural levels, probably at depths less than ca. 7 km. Thus, D_3 extension is not prone for having supported large parts of the exhumation due to tectonic denudation. Nevertheless, the way-up jump in metamorphic grade from anchizone to the diagenesis–anchizone transition in the upper violet slates might be related to extensional shearing. This jump also explains why the semibrittle D_3 structures are entirely lacking in the upper part of the upper violet slates where the D_3 stage must have occurred under more brittle conditions that led to steep cataclastic normal faults, which are similar to those of D_5.

D_3 crustal extension was interrupted by a further phase of N–S compression that led to D_4 brittle folding and related top-to-the-S thrusting associated with moderate crustal thickening. This observation is not in line with Jolivet et al. (1996), who claimed that the entire post-peakmetamorphic strain is related to extension and exhumation below the 'crustal-scale detachment' at the boundary between the PQU and the Tripolitza unit. Although the D_4 thrusts are of the brittle type, D_4 folds in metapelitic rocks are accompanied by an axial-plane solution cleavage suggesting that temperature and lithostatic pressure during D_4 were still above critical values where pressure solution was active (ca. 200 °C and 5–7 km depth according to Holl and Anastasio (1995)). D_4 led to kilometer-scale E–W to ENE–WSW trending syn- and antiforms, which predate the deposition of the middle Miocene sediments. The large scattering of D_4 fold axes probably results from the pre-existing D_2 fold axes, which may have formed a bending anisotropy

that influenced the orientation of D_4 fold axes (e.g. Cobbold and Watkinson, 1981).

The D_4 folding and thrusting was succeeded by D_5 high-angle normal faulting, that reflect N–S extension and subsequent D_6 strike-slip movements, probably due to N–S compression.

7. Conclusions

The Alpine tectonometamorphic evolution of the PQU of eastern Crete is characterized by several phases of N–S compression and N–S extension that led to a complex tectonostratigraphic sequence. Discontinuities in protolith age and in metamorphic grade of this sequence can be attributed to both crustal thickening, due to D_2 and D_4 thrusting, and crustal extension, due to D_3 semibrittle normal faulting. The multiple changes from compression to extension, starting with subduction/collision at the Oligocene/Miocene boundary and lasting until recent times, is not compatible with a retreating plate boundary and permanent 'roll back' of the Hellenic subduction zone since the late Eocene, as is suggested by Thomson et al. (1998b).

The major crustal-scale detachment of Fassoulas et al. (1994) and Jolivet et al. (1996) is situated within the upper part of the PQU, whereas the contact between the PQU and the overlying Tripolitza unit could also represent a brittle D_4 top-to-the-S thrust contact, as has been suggested by Wachendorf et al. (1975). To answer this question, similar investigations like those of the present study should be applied to the Tripolitza carbonates. Moreover, further investigations are needed to explain the significant difference in subduction-related strain geometry and rheology between eastern and western Crete. These differences can partly be explained by the difference in metamorphic peak temperature that is ca. 100 °C (see above). The dominance of flattening strain in the PQU of western Crete (Stöckhert et al., 1999) might result from enhanced solution–precipitation creep and related volume loss at $T =$ ca. 400 °C. However, although the differential stresses are expected to be lower at higher temperatures, there is no reason why the more deeply subducted rocks of western Crete should not have recorded evidence for higher differential stresses at higher structural levels. During progressive subduction, the high-pressure, low-temperature metamorphic rocks of western Crete should have passed the high-stress structural level that is now exposed in eastern Crete.

Acknowledgements

We are grateful to N. Ibrahimi (Frankfurt), S. Krumm and A. Weh (Erlangen) for preparing parts of the IC samples. Thanks also to Th. Doutsos (Patras) and to IGME (Athens) who provided topographic maps of eastern Crete. We further acknowledge the helpful reviews by L. Jolivet and U. Ring. This study was supported by Deutsche Forschungsgemeinschaft (DFG-Schwerpunktprogramm ICDP/KTB, grant Zu 73/5).

References

Andersen, T.B., Jamtveit, B., 1990. Uplift of deep crust during orogenic extensional collapse: a model based on field studies in the Sogn–Sunnfjord region of western Norway. Tectonics 9, 1097–1111.

Burkhard, M., 1993. Calcite twins, their geometry, appearance and significance as stress-strain markers and indicators of tectonic regime: a review. J. Struct. Geol. 15, 351–368.

Cobbold, P.R., Watkinson, A.J., 1981. Bending anisotropy: a mechanical constraint on the orientation of fold axes in an anisotropic medium. Tectonophysics 72, T1–T10.

Creutzburg, N., Seidel, E., 1975. Zum Stand der Geologie des Präneogens auf Kreta. N. Jb. Geol. Paläont. Abh. 149, 363–383.

Dallmeyer, R.D., Takasu, A., 1992. $^{40}Ar/^{39}Ar$ ages of detrital muscovite and whole-rock slate/phyllite, Narragansett basin, Ri-MA, USA: implications for rejuvenation during very low-grade metamorphism. Contrib. Mineral. Petrol. 110, 515–527.

Dornsiepen, U.F., Manutsoglu, E., 1994. Zur Gliederung der Phyllit–Decke Kretas und des Peloponnes. Z. dt. geol. Ges. 145, 286–304.

Duyster, J., 1991. Strukturgeologische Untersuchungen im Moldanubikum (Waldviertel, Österreich) und methodische Untersuchungen zur bildanalytischen Gefügequantifizierung von Gneisen. Ph.D. thesis, Univ. Göttingen, Germany, 141pp.

Erslev, E.A., 1988. Normalized center-to-center strain analysis of packed aggregates. J. Struct. Geol. 10, 201–209.

Etchecopar, A., Malavieille, J., 1987. Computer models of pressure shadows: a method for strain measurements and shear-sense determination. J. Struct. Geol. 9, 667–677.

Etheridge, M.A., Wilkie, J.C., 1981. An assessment of dynamically recrystallized grainsize as a paleopiezometer in quartz-bearing mylonite zones. Tectonophysics 78, 475–508.

Fassoulas, C., Kilias, A., Mountrakis, D., 1994. Postnappe stacking extension and exhumation of high-pressure/low-temperature rocks in the island of Crete, Greece. Tectonics 13, 127–238.

Ferreiro Mählmann, R., 1994. Zur Bestimmung von Diagenesehöhe und beginnender Metamorphose-Temperaturgeschichte und Tektogenese des Austroalpins und Südpenninikums in Voralberg und Mittelbünden. Frankfurter geowiss. Arb. C 14, 1–498.

Franz, L., 1992. Die polymetamorphe Entwicklung des Altkristallins auf Kreta und im Dodekanes (Griechenland). Ferdinand Enke, Stuttgart 389pp.

Frey, M., 1988. Discontinuous inverse metamorphic zonation, Glarus Alps, Switzerland: evidence from illite 'crystallinity' data. Schweizerische Mineralogisch Petrographische Mitteilungen 68, 171–183.

Fry, N., 1979. Random point distributions and strain measurement in rocks. Tectonophysics 60, 89–105.

Gleason, G.C., Tullis, J., 1993. Improving flow laws and piezometers for quartz and feldspar aggregates. Geophys. Res. Lett. 20, 2111–2114.

Gleason, G.C., Tullis, J., 1995. A flow law for dislocation creep in quartz aggregates determined with the molten salt cell. Tectonophysics 247, 1–23.

Greiling, R., 1982. The metamorphic and structural evolution of the Phyllite–Quartzite nappe of western Crete. J. Struct. Geol. 4, 291–297.

Guillope, M., Poirier, J.P., 1979. Dynamic recrystallization during creep of single-crystalline halite: an experimental study. J. Geophys. Res. 84, 5557–5567.

Haude, G., 1989. Geologie der Phyllit-Einheit im Gebiet um Palekastro (Nordost-Kreta, Griechenland). Ph.D. thesis, Technical University Munich, Germany, 131pp.

Hirth, G., Tullis, J., 1992. Dislocation creep regimes in quartz aggregates. J. Struct. Geol. 14, 145–159.

Hoeppener, R., 1955. Tektonik im Schiefergebirge. Geol. Rundsch. 44, 26–58.

Holl, J.E., Anastasio, D.J., 1995. Cleavage development within a foreland fold and thrust belt, southern Pyrenees, Spain. J. Struct. Geol. 17, 357–369.

Jaoul, O., Tullis, J., Kronenberg, A., 1984. The effect of varying water content on the behaviour of Heavitree quartzite. J. Geophys. Res. 89, 4298–4312.

Jolivet, L., Goffé, B., Monié, P., Truffert-Luxey, C., Patriat, M., Bonneau, M., 1996. Miocene detachment in Crete and exhumation *P–T–t* paths of high-pressure metamorphic rocks. Tectonics 15, 1129–1153.

Kilias, A., Fassoulas, C., Mountrakis, D., 1994. Tertiary extension of continental crust and uplift of Psiloritis metamorphic core complex in the central part of the Hellenic Arc (Crete, Greece). Geol. Rundsch. 83, 417–430.

Koch, P.S., 1983. Rheology and microstructures of experimentally deformed quartz aggregates. Ph.D. thesis, Univ. Calif., Los Angeles, 464pp.

Kozur, H., Krahl, J., 1987. Erster Nachweis von Radiolarien im tethyalen Perm Europas. N. Jb. Geol. Paläont., Abh. 174, 357–372.

Krahl, J., Kauffmann, G., Richter, D., Kozur, H., Möller, I., Förster, O., Heinritzi, F., Dornsiepen, U., 1986. Neue Fossilfunde in der Phyllit-Gruppe Ostkretas (Griechenland). Z. dt. geol. Ges. 137, 523–536.

Kronenberg, A.K., Tullis, J., 1984. Flow strengths of quartz aggregates: Grain size and pressure effects due to hydrolytic weakening. J. Geophys. Res. 89, 4281–4297.

Küster, M., Stöckhert, B., 1997. Density changes of fluid inclusions in high-pressure low-temperature metamorphic rocks from Crete: a thermobarometric approach based on the creep strength of the host minerals. Lithos 41, 151–167.

Le Pichon, X., Lyberis, N., Angelier, J., Renard, V., 1982. Strain distribution over the East Mediterranean Ridge; a synthesis incorporating new Sea-Beam data. Tectonophysics 86, 243–274.

Lister, G.S., Banga, G., Feenstra, A., 1984. Metamorphic core complexes of Cordilleran type in the Cyclades, Aegean Sea, Greece. Geology 12, 221–225.

Mercier, J.C., Anderson, D.A., Carter, N.L., 1977. Stress in the lithosphere. Inferences from steady state flow of rocks. Pure Appl. Geophys. 115, 119–126.

Meulenkamp, J.E., Wortel, M.J.R., van Wamel, W.A., Spakman, W., Hoogerduynstrating, E., 1988. On the Hellenic subduction zone and the geodynamic evolution of Crete since the late Middle Miocene. Tectonophysics 146, 203–215.

Nadai, A., 1963. Theory of Flow and Fracture of Solids. McGraw Hill, New York.

Ord, A., Christie, J.M., 1984. Flow stresses from microstructures in mylonitic quartzites of the Moine thrust zone, Assynt area, Scotland. J. Struct. Geol. 6, 639–654.

Paterson, M.S., Luan, F.C., 1990. Quartzite rheology under geological conditions. In: Knipe, R.J., Rutter, E.H. (Eds.). Deformation mechanisms, rheology and tectonics. Geol. Soc. Spec. Publ. 45, 299–307.

Peach, C.J., Lisle, R.J., 1979. A Fortran IV program for analysis of tectonic strain using deformed elliptical markers. Comput. Geosci. 5, 325–334.

Ramsay, J.G., 1980. The crack-seal mechanism of rock deformation. Nature 284, 135–139.

Ramsay, J.G., Wood, D.S., 1973. The geometric effects of volume change during deformation processes. Tectonophysics 16, 263–277.

Ramsay, J.G., Huber, M.I., 1983. The Techniques of Modern Structural Geology. Vol. 1: Strain Analysis. Academic Press, London 307pp.

Ramsay, J.G., Huber, M.I., 1987. The techniques of modern structural geology, Vol. 2: Folds and Fractures. Academic Press, London, 700 pp.

Rowe, K.J., Rutter, E.H., 1990. Paleostress estimations using calcite twinning: experimental calibration and application to nature. J. Struct. Geol. 12, 1–17.

Rutter, E.H., 1976. The kinetics of rock deformation by pressure solution. Phil. Trans. Roy. Soc. A283, 203–219.

Schwarz, S., Stöckhert, B., 1996. Pressure solution in siliciclastic HP–LT metamorphic rocks–constraints on the state of stress in deep levels of accretionary complexes. Tectonophysics 255, 203–210.

Seidel, E., Okrusch, M., Kreuzer, H., Raschka, H., Harre, W., 1981. Eo-Alpine metamorphism in the uppermost unit of the Cretan nappe system, petrology and geochronology. Contrib. Mineral. Petrol. 76, 351–361.

Seidel, E., Kreuzer, H., Harre, W., 1982. A Late Oligocene/Early Miocene high pressure belt in the external Hellenides. Geol. Jb. E 23, 165–206.

Sibson, R.H., Moore, J.M., Rankin, A.H., 1975. Seismic pumping—a hydrothermal fluid transport mechanism. J. Geol. Soc. London 131, 653–659.

Soujon, A., Jacobshagen, V., 1997. Illit-Kristallinitäten in der Plattenkalk-Gruppe Kretas. Abstract of ICDP/KTB-Kolloquium, Ruhr-Universität Bochum, Germany.

Stöckhert, B., Wachmann, M., Küster, M., Bimmermann, S., 1999. Low effective viscosity during high pressure metamorphism due to dissolution precipitation creep: the record of HP–LT metamorphic carbonates and siliciclastic rocks from Crete. Tectonophysics 303, 299–319.

Stüben, D., Berner, Z., 1999. Fluidhaushalt und Stofftransportprozesse im Akkretionskomplex von Kreta (Griechenland). Abstract of ICDP/KTB-Kolloquium, Ruhr-Universität Bochum.

Taymaz, T., Jackson, J., McKenzie, D., 1991. Active tectonics of the north and central Aegean Sea. Geophys. J. Int. 106, 433–490.

Theye, T., Seidel, E., 1991. Petrology of low-grade high-pressure metapelites from the External Hellenides (Crete, Peloponnese). A case study with attention to sodic minerals. Eur. J. Mineral. 3, 343–366.

Theye, T., Seidel, E., 1993. Uplift-related retrogression history of aragonite marbles in Western Crete (Greece). Contrib. Mineral. Petrol. 114, 349–356.

Theye, T., Seidel, E., Vidal, O., 1992. Carpholite, sudoite and chloritoid in low-temperature high-pressure metapelites from Crete and the Peloponnese, Greece. Eur. J. Mineral. 4, 487–507.

Thomson, S.N., Stöckhert, B., Rauche, H., Brix, M.R., 1998a. Apatite fission-track thermochronology of the uppermost tectonic unit of Crete, Greece: implications for the post-Eocene tectonic evolution of the Hellenic subduction system. In: van den Haute, P., de Corte, F. (Eds.). Advances in Fission-track Geochronology. Kluwer Academic Publishers, Dortrecht, pp. 187–205.

Thomson, S.N., Stöckhert, B., Brix, M.R., 1998b. Thermochronology of the high-pressure metamorphic rocks of Crete, Greece: implications for the speed of tectonic processes. Geology 26, 259–262.

Twiss, R.J., 1977. Theory and applicability of a recrystallized grain size paleopiezometer. Pure Appl. Geophys. 115, 225–244.

Twiss, R.J., 1980. Static theory of size variation with stress for subgrains and dynamically recrystallized grains. U.S. Geol. Survey, Open File Repository, 80-625, pp. 665–683.

Twiss, R.J., Moores, E.M., 1992. Structural Geology. W.H. Freeman & Co, New York 532pp.

Unzog, W., 1990. Beispiele von Strainanalysen in Kristallingebieten. Extended abstract of 3rd Symposium für Tektonik, Strukturgeologie, Kristallingeologie (TSK III), Graz, Austria, pp. 265–266.

Wachendorf, H., Best, G., Gwosdz, W., 1975. Geodynamische Interpretation Ostkretas. Geol. Rundsch. 64, 728–750.

White, S.H., 1979. Grain and sub-grain size variations across a mylonite zone. Contr. Miner. Petrol. 70, 193–202.

Wortel, M.J.L., Goes, S.D.B., Spakman, W., 1993. Structure and seismicity of the Aegean subduction zone. Terra Nova 2, 554–562.

Xypolias, P., Doutsos, T., 2000. Kinematics of rock flow in a crustal-scale shear zone: implication for the orogenic evolution of the southwestern Hellenides. Geol. Mag. 137, 81–96.

Zulauf, G., 1997. Constriction due to subduction: evidence for slab pull in the Mariánské Lázne complex (central European Variscides). Terra Nova 9, 232–236.

Zulauf, G., 2001. Structural style, deformation mechanisms and paleostress along an exposed crustal section: constraints on the rheology of quartzofeldspathic rocks at supra- and infrastructural levels (Tepla Barrandian unit, Bohemian Massif). Tectonophysics 332, 211–237.